applied sciences

MDPI

Article

An Adaptive and Scalable Protection Coordination System of Overcurrent Relays in Distributed-Generator-Integrated Distribution Networks

Duong Minh Bui [1,*], Phuc Duy Le [2,3], Thanh Phuong Nguyen [3] and Hung Nguyen [3]

[1] Department of Electrical and Computer Engineering (ECE), Faculty of Engineering, Vietnamese-German University (VGU), Thu Dau Mot City 75000, Vietnam
[2] Department of Administration, Ho Chi Minh City Power Corporation, Ho Chi Minh City 70000, Vietnam; phucld91@gmail.com
[3] HUTECH Institute of Engineering, Ho Chi Minh City University of Technology (HUTECH), Ho Chi Minh City 70000, Vietnam; nt.phuong@hutech.edu.vn (T.P.N.); n.hung@hutech.edu.vn (H.N.)
* Correspondence: duong.bm@vgu.edu.vn; Tel.: +84-918-163-356

Abstract: Integration of distributed generators (DGs) into a distribution network (DN) can cause coordination challenges of overcurrent relays (OCRs) because of different fault-current contributions of DGs as well as the directional change in fault currents. Therefore, the OCRs should be properly coordinated to maintain their adaptability and scalability to protect the DG-integrated distribution network. In this study, an adaptive and scalable protection coordination (ASPC) approach has been developed for the OCRs in a DG-contained distribution network based on two implementation stages. At the first stage, the reliability improvement of fault-current calculation results is performed by determining the min-max confidence interval of fault current for each different fault type, which is the basis for properly selecting tripping and pick-up thresholds of definite-time and inverse-time OC functions in the same OCR. At the second stage, optimization algorithms are used for calculating protection-curve coefficients and Time-Dial Setting (TDS) multiplier for the inverse-time OC functions in the OCR. A real 22 kV DG-integrated distribution network which is simulated by ETAP software is considered a reliable test-bed to validate the proposed ASPC system of OCRs in the multiple-DG-contained distribution network. In addition, the coordination results of OCRs can be obtained by three common optimization algorithms, Particle Swarm Optimization (PSO), Gravitational Search Algorithm (GSA), and Genetic Algorithm (GA). These relay coordination results have shown an effective protection combination of the definite-time OC functions (50P and 50G) and the inverse-time OC functions (51P and 51G) in the same OCR to get the adaptable and scalable DN protection system.

Keywords: distributed generator; distribution network; overcurrent relay; fault protection; relay coordination; meta-heuristic algorithms

Citation: Bui, D.M.; Le, P.D.; Nguyen, T.P.; Nguyen, H. An Adaptive and Scalable Protection Coordination System of Overcurrent Relays in Distributed-Generator-Integrated Distribution Networks. *Appl. Sci.* **2021**, *11*, 8454. https://doi.org/10.3390/app11188454

Academic Editors: Federico Barrero and Mario Bermúdez

Received: 26 August 2021
Accepted: 9 September 2021
Published: 12 September 2021

1. Introduction

1.1. Motivation and Assumption

Distributed generators have been recently developed to utilize sustainable and clean energy sources for electrical energy conversion. DGs can operate as ancillary services to improve power-supply reliability indices, SAIFI (System Average Interruption Frequency Index) and SAIDI (System Average Interruption Duration Index), to a distribution network. However, the operation characteristics of DGs could lead to certain difficulties in an overcurrent protection system of DN because of the remarkable change in fault-current values observed by overcurrent relays (OCRs). Specifically, fault-current values depend on DG types, locations, and technologies. For example, rotating-based distributed generators (RBDGs) can contribute high fault currents whereas inverter-based distributed generators (IBDGs) can only inject the limited fault currents about 1.2~2.0 p.u. to a distribution network [1–3]. Moreover, high penetration of DGs may lead to a magnitude

decrease in fault-currents contributed from the utility, which can reduce the sensitivity and selectivity of OCRs on feeders of the distribution network [4–8]. Malfunction issues of OCRs in the DG-integrated DN could be over-reach or under-reach of OC relays, loss of sensitivity/selectivity, blinding of overcurrent protection, false tripping or sympathetic tripping of overcurrent protection [9].

Several studies are performed on protection coordination of overcurrent relays in a DG-integrated DN. In [10], risks of protection miscoordination of OCRs or reclosers are indicated in each fault isolation and service restoration (FISR) plan when the DN needs to change its topology due to faulted events. In [11], the authors point out that the allowable fault-current contribution of IBDGs can significantly impact a DN's overcurrent protection system. In [12–15], the threshold setting of OCRs is only valid for typical DG capacities. In [16], the authors have introduced a hybrid PSO-based protection coordination method to adjust TDS parameters of directional overcurrent relays. The paper [17] proposed an optimization function to calculate tripping and pick-up thresholds of OCRs in a range of pre-defined values. In [18], an adaptive overcurrent protection system is developed for fault detection and isolation in a DG-penetrated distribution network. The research paper [19] has proposed an ANN-based method to divide a distribution network into multiple zones, and then an overcurrent protection scheme for each zone is developed. In [20], an effective overcurrent protection system is developed to protect a distribution network when considering two on-grid and off-grid operation modes of DGs. From the above references, it could be generally concluded that the accurate calculation of fault-current values can strongly impact the protection coordination results of OCRs on a DN having DGs. That assumption could be more considered in this study by contributing a novel proposal to determine the min-max confidence interval of fault currents according to each different fault type. The estimated confidence interval of fault currents will then be the basis for properly selecting tripping and pick-up thresholds of the OCRs in the DN.

The DG-integrated distribution networks mostly use digital relays with overcurrent and sequence-component-based protection functions. Accordingly, overcurrent-based protection functions, e.g., 50, 51, 67, or sequence-component-based protection functions, e.g., 46, 47, 50REF, 46BC, $3I_0$, $3V_0$, can be properly re-adjusted when the topology of DN is changed under fault events. As presented in [18], a low-voltage microgrid (LVMG) protection system using directional overcurrent protection functions in digital relays is developed along with its coordination strategies. The paper [21] presents a protection coordination solution based on symmetrical and differential current components to detect faults in a grid-connected microgrid. In [22], the authors propose a definite-time overcurrent protection model regarding the placement of DGs in a distribution network. In [23], a novel protection coordination algorithm is developed to improve the selectivity of the protection system through using a three-level communication network, directional overcurrent protection functions, and under/overvoltage-based protection functions, which are available in digital relays. On the other hand, references [24,25] have considered sequence-component-based protection functions, e.g., positive-, negative-, zero-sequence components, along with a GOOSE (Generic Object Oriented System Event) solution for detecting, classifying and isolating symmetrical and asymmetric faults in microgrids or DG-penetrated distribution networks. Generally, embedding several different protection functions into a digital relay could be a feasible solution to improve the adaptability and flexibility of a DN protection system, which has been applied for this study.

1.2. Literature Review

Protection coordination of OCRs in a distribution network is severely affected by the presence of DGs [9]. According to different DG penetration levels, DG sites, and fault types and locations in the DN, determining the optimal setting values of pick-up current, TPS multiplier, and inverse-time curve coefficients of overcurrent relay is very necessary to ensure the adaptability and reliability of a DN protection system. Many coordination methods of overcurrent relays can be classified by trial-and-error methods [26], topological

analysis methods [27], and optimization methods [28–30]. The latter is commonly used in recent years because the operating time of OC relays can be optimized against various coordination constraints as well as relay characteristic curves. The optimal coordination of overcurrent relays consists of an objective function (OF), parameters, constraints and a selected optimization method to solve the defined problem. A literature survey for the objective functions with parameters and constraints, type of OC relays, and optimization algorithms has been shown as the following.

- Objective function and setting parameters: In [29–36], objective functions are based on the overall operation time of primary and back-up overcurrent relays, where time-dial setting (TDS) multipliers are considered as the optimized parameters. In [37–50], the optimized parameters of OFs are pick-up currents or both the pick-up currents and TDS multipliers. In [51,52], a multi-objective function (MOF) with the overall operation time of relays and protection coordination constraints has been developed. The optimization parameters of the MOF are TDS multipliers, pick-up currents and coefficients of time-current characteristic curves. In [52], the authors have explained why adaptive coordination schemes are paid more attention to an overcurrent protection system of the DG-integrated DN when compared to others such as: immediate disconnection of DGs under a fault event; capacity limitation of installed DGs; protection system improvement by using more circuit breakers for sectionalization, distance relays, or directional OC relays (DOCRs); the use of fault current limiters to preserve the original settings of OC relays; and the use of fault ride through (FRT) strategies of inverter-based DGs. Based on the references [15,19,42,43], an adaptive protection coordination (APC) scheme must first update the data from the latest change of DG-integrated distribution network, e.g., the operation status of DGs, the opened/closed status of circuit breakers (CBs), and then calculate power flows and perform the fault analysis to obtain the input data for optimal coordination algorithms. The APC scheme could require a data center to send/receive the data to/from digital relays before or after the sudden changes/disturbances of the DG-penetrated DN. A supervisory control and data acquisition (SCADA) system is needed to perform this adaptive coordination scheme. Moreover, digital relays can be remotely controlled through communication channels. According to the above references, the combination of digital relays, the SCADA system, and an appropriate optimization algorithm will be necessary for the adaptive coordination of OCRs in the DG-integrated DN. The optimal settings of both TDS multipliers and protection-curve coefficients for the inverse-time OC function could be easily implemented in a digital relay. Furthermore, several previous studies have not considered both the reliability of fault-current calculation results and the proper selection of tripping and pick-up thresholds of OCRs in the DN for the optimization of the objective function. Last but not least, it is needed to consider the operation characteristics of DG units, e.g., plug-and-play, peer-to-peer characteristics [53–55], for parameter settings of the adaptable relay coordination system in the DG-contained DN.
- Type of OC relays: In [29,39,40], the optimal coordination of non-directional OC relays has been considered. In [12,56], different operation characteristic curves of non-directional OC relays have been analyzed in detail. The OC relays can be classified into three main types: instantaneous, definite-time, and inverse-time OC relays. If the measured current exceeds a tripping-current threshold, the instantaneous OC relay sends a tripping signal immediately to circuit breakers, while the definite-time overcurrent relay will send a trip signal after a pre-defined time-delay. The inverse-time OC relay operates with a typically mathematical function with certain parameters to form a protection curve as followed by IEC 60255-3 or IEEE C37.112-2018 standards [57,58]. The optimal coordination algorithm of OC relays usually focuses on the inverse-time function. In [59,60], the admittance-based inverse-time OC relay is used to improve the sensitivity of fault detection in the DN and microgrids. In [61–64], the voltage-based inverse-time OC relay is used to be more sensitive to different

fault types and reduce the total operation time of relays. In [65], the single and dual settings of OC relays are proposed to increase the selectivity of the protection system under the high penetration of DGs into the DN. In general, the above-mentioned works only consider the inverse-time OC function as an objective function to be optimized, however, it can be proposed to combine the definite-time OC function with the inverse-time OC function to protect a DG-based distribution network. The reference [66] has solved this research gap, but how to demonstrate the reliability of calculated fault-current values in the DG-integrated distribution network has not been paying attention to. In fact, minimum and maximum fault-current values of each fault type are the basis to properly set-up the inverse-time and define-time OC functions in the protection system.

- Coordination algorithms of OC relays: In [39,54], two PSO (Particle Swarm Optimization) and GS (Gravitational Search) algorithms are used to calculate TDS multipliers and pick-up currents for the OC relays in a DG-contained DN. In [53], a microgenetic algorithm is used to calculate overcurrent protection settings under any change in the DN configuration. In [66], a Firefly Algorithm (FA) is applied to coordinate the definite-time OC functions and the inverse-time OC functions in the DN protection system. In [67], a continuous genetic algorithm (CGA) is used for the optimal coordination of OC relays in a ring-type distribution system. In [68], the Firefly and Chaotic Firefly algorithms have been applied to solve the coordination problem of OC relays. In [69], a modified PSO algorithm is proposed to calculate the optimal relay settings. Generally, the main objective of coordination algorithms is to achieve the possible minimum tripping times through the optimal parameter settings of each OC relay. Typically, this study proposes to use three very common techniques such as GA, GSA, and hybrid PSO-GSA (Gravitational Search Algorithm) to calculate the TDS multiplier and inverse-time curve coefficients for each OC relay in a DG-contained distribution network. To explain that, the GA is a well-known optimization algorithm, whereas the GSA and the hybrid PSO-GSA are recently developed and also applied for protection coordination of OC relays in the DG-contained DN because of high convergence to the global optimal solution with several different constraints [39]. Moreover, relay coordination results of the GA can be used as the standard results to compare with the results of the GSA and the hybrid PSO-GSA.
- Directional OC (DOC) relays and coordination algorithms: In [17,24,44–46,48–50], the optimal coordination of DOC relays in the distribution network has been performed. Reference [17] uses a simplex algorithm to solve the protection coordination of DOC relays as a linear programming problem. References [24,42] use a differential evolution (DE) algorithm for the optimal coordination of bi-directional OC relays in the closed-loop distribution networks. In [31], a non-dominated sorting genetic algorithm-II (NSGA-II) is proposed for the coordination of DOC relays to minimize the total operating time of primary and backup relays with a multi-objective function. More recently, heuristic techniques, such as Cuckoo optimization algorithm [38], Electromagnetic Field Optimization (EFO) algorithm [41], the Hybrid GA-NLP Approach [44], evolutionary algorithm and linear programming [45], a biogeography-based optimization (BBO) algorithm [46], Symbiotic Organism Search Optimization technique [48], seeker algorithm [49], ant colony optimization (ACO) [43], bee colony optimization (BCO) [70], an Imperialistic Competition Algorithm [71], teaching learning-based optimization (TLBO) [72], harmony search algorithm [73], or firefly algorithm [74] are also used as powerful tools to solve the optimization coordination problem of DOC relays in the distribution network. In general, it can be concluded that many recent studies on coordination algorithms are performed for DOC relays in a DG-integrated distribution network because the presence of DGs leads to the directional change of fault currents. The operation characteristic of DOC relays is similar to that of OC relays excepting for the directional-change detection of fault currents [75–80]. In conclusion, it should be noted that the purpose of this survey is to provide a more comprehensive

view of many recent protection coordination algorithms for DOC relays in the DN. The directional-change detection functions of fault currents are out of the research scope so that this study will only focus on the development of an adaptive and scalable protection coordination system of overcurrent relays in a DG-integrated DN.

1.3. Contributions and the Paper Structure

According to an aforementioned literature survey, it is needed to develop an adaptive and scalable protection coordination (ASPC) approach for OCRs in the DG-integrated DN to improve the reliability of protection system. The ASPC approach for OCRs has two main performance stages: (i) Stage I–increasing the reliability of fault-current calculation results and selecting tripping and pick-up current thresholds for the OCRs; and (ii) Stage II–applying the optimization algorithms to calculate the coefficients and Time-Dial-Setting (TDS) multiplier for the inverse-time OC functions in the OCR. More clearly, Stage I finds the min-max confidence interval of fault currents for each different fault type (e.g., 3ph-G fault, 2ph-G fault, 1ph-G fault, and ph-ph fault) which is the basis for properly selecting tripping and pick-up thresholds of definite-time and inverse-time OC functions in the same OCR. Stage II uses three common optimization algorithms, Particle Swarm Optimization (PSO), Gravitational Search Algorithm (GSA), and Genetic Algorithm (GA) to determine the coefficients and TDS multiplier for the inverse-time OC functions. The objective function of the ASPC approach for the OCRs is formulated by three certain constraints consisting of Coordination Time Interval (CTI), relay operating time and TDS multiplier. Novel contributions and assumptions related to the ASPC system of the OC relays are briefly shown as follows:

- Increasing the reliability of fault-current calculation results: According to the literature survey, either nominal bus-voltage values or voltage values calculated right after some pre-determined cycles are commonly considered as the reference voltages for the power-flow analysis and fault-current calculation. However, the use of nominal bus-voltage values could lead to inaccurate calculations of power flows and fault currents in the distribution network, which can result in the protection miscoordination of OCRs. Therefore, this study will propose a novel statistical data-filtering method to determine a min-max confidence interval of load power $[P_{\text{load\_min}}, P_{\text{load\_max}}]$ and load current $[I_{\text{load\_min}}, I_{\text{load\_max}}]$ at each load bus in the DN, as referred in Sections of Forecasting a Min-Max Confidence Interval of Load Power at Each Load Bus and Calculating a Min-Max Confidence Interval of Load Current at Each Load Bus, respectively. Next, a current-injection-based power-flow (CIBPF) analysis method is used to calculate the min-max confidence interval of bus voltage at any i-th bus on the DN, $[V_{i\_\text{min}}, V_{i\_\text{max}}]$ instead of using either the nominal bus-voltage values or the voltage values calculated right after some pre-determined cycles from the power-flow analysis, as referred to Section of The Current-Injection-Based Power Flow Analysis. Based on the confidence intervals of bus-voltages in the distribution network, an adaptable fault analysis technique depicted in Section of An Adaptable Fault Analysis Technique is proposed to calculate the min-max confidence intervals of fault currents contributed by different DG units and fault current contributed by the utility which are used for effectively selecting tripping and pick-up thresholds of definite-time and inverse-time OC functions in the same OCR. In other words, instead of using a fixed fault-current value for each fault type with the unconsidered reliability, this paper has contributed an adaptable fault analysis technique to calculate the min-max confidence interval of fault current. The maximum and minimum confidence thresholds of fault current are then used to select tripping and pick-up thresholds of definite-time and inverse-time OC functions, respectively.
- Propose to use both definite-time and inverse-time protection functions in the same OCR to protect a DG-based distribution network.

- Propose to use the SCADA system to update the operation status of DGs and the opened/closed status of circuit breakers (CBs), and to remotely control digital relays for the ASPC approach.
- The ASPC system of OCRs can be effectively operated regarding different fault scenarios in the DG-based distribution system as well as the 'on-grid' or 'off-grid' operation modes for DG units in the DN.
- A real 22 kV DG-integrated distribution network which is simulated by ETAP software considered to be a reliable test-bed to validate the proposed ASPC system of OCRs.
- Coordination results of the OCRs are based on three optimization algorithms, Particle Swarm Optimization (PSO), Gravitational Search Algorithm (GSA) and Genetic Algorithm (GA), as referred in Section 2.4.

The remaining sections of the paper are organized as follows. Section 2 presents the proposed ASPC approach for OCRs in the DG-based DN. This section presents an objective function of OCR protection coordination, coordination constraints of the OCRs in the DN, the reliable and accurate calculation method of minimum and maximum fault currents for each fault type in the DN having DGs, selection of pick-up and tripping currents for OCRs, and three common optimization algorithms, GSA, hybrid PSO-GSA and GA. Section 3 describes a case study of the practical 22 kV DG-integrated distribution network. Section 4 indicates the optimal protection coordination results of OCRs in the practical 22 kV DN, analysis and discussion on these relay coordination results. Last but not least, Section 5 contains the conclusions of the study.

2. A Proposed ASPC Approach for OCRs in a DG-Integrated Distribution Network

2.1. Modelling of OC Relay Characteristics

In this study, the definite-time OC functions (e.g., 50P for the phase-to-phase fault protection; 50G for the ground fault protection) are deployed as primary protection, while the inverse-time OC functions (e.g., 51P for phase-to-phase fault protection and 51G for ground fault protection) are used for both primary and backup protection. Parameter settings of definite-time and inverse-time OC functions are separate; however, it always allows that the primary protection is activated before the backup protection. The IEEE C37.112^{TM}-2018 standard characteristics are considered for the relay coordination problem [57,58]. The operating time equation of the standard inverse-time OC function is given by Equation (1):

$$T_{F51\_ik} = TDS_i \left[\frac{A}{\left(I_{f\_ik} / I_{pu\_i} \right)^{B} - 1} + C \right] \quad (1)$$

where T_{F51_ik} is the operation time of the i-th relay (R_i) for a k fault location in the protected line/zone of the distribution network; TDS_i and I_{pu_i} are the time dial setting (TDS_i) and pick-up current (I_{pu_i}) parameters of the i-th relay, respectively; I_{f_ik} is the fault current seen by the i-th relay for the fault at k location; and A, B, and C are the coefficients of the inverse-time protection curve. Figure 1 illustrates the protection characteristic curves of definite-time (50) and inverse-time (51) OC functions.

2.2. Objective Function of Overcurrent Protection Coordination

The objective is to find the optimal value of TDS_i and three A, B, and C coefficients of each OCR, while I_{pu_i} and I_{f_ik} are properly selected from fault analysis results of the DG-based distribution network. The coordination problem of OCRs is to minimize the total operating time of all relays working as the primary protection but still satisfying certain constraints and maintaining the reliability of the protection system. The objective function is expressed by Equation (2) as follows:

$$\min Z = \sum_{i=1}^{n} T_{F51\_ik,pri} \quad (2)$$

where n is the total number of relays; and $T_{F51\_ik,pri}$ is the operating time of the i-th OC relay at the k faulted location working as the primary protection. This study proposes to only consider one faulted point/location for each protected line/zone, normally at the remote end of the protected line/zone where the minimum fault current can be calculated as the basis to select a pick-up current threshold for the primary OC relay of this protected line/zone in the distribution network, as referred to Section 2.3.4.

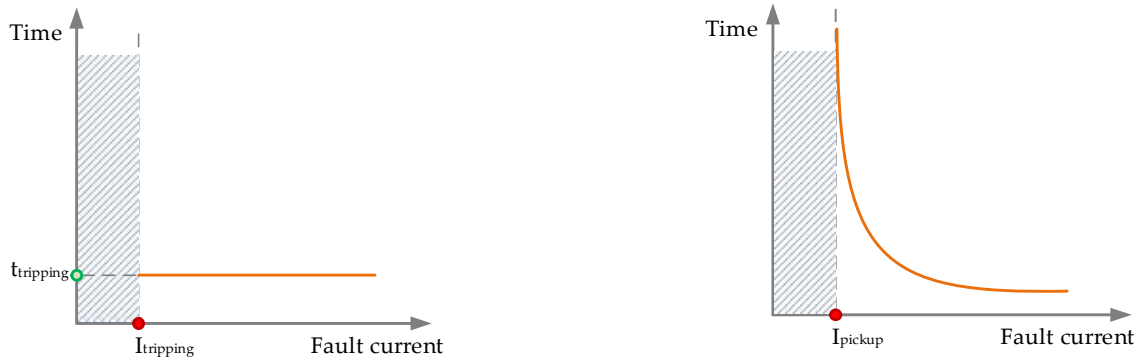

$I_{tripping}$-a tripping-current threshold of the OC relay

(**a**)

$I_{pick-up}$-a pick-up current threshold of the OC relay

(**b**)

Figure 1. Illustration of protection characteristic curves (**a**) 50P/G–definite-time overcurrent function and (**b**) 51P/G–inverse-time overcurrent function.

On the other hand, it is most common to use the OCR pairs, e.g., one primary relay and one backup relay for each OCR pair, to detect and clear a given fault in the protected line/zone. However, to improve the scalability and selectivity of an overcurrent relay coordination system in the DN having DGs, this study proposes to use the OCR triples, i.e., one for the primary relay and two other consecutive ones for the backup relays. The total tripping time of the OCR triple is formulated as follows:

- For the upward direction of fault current to the relay R_i:

$$2 * \mathrm{CTI}^{\min} \leq t_{F51,(upward-upward-i)k,backup} + t_{F51,(upward-i)k,backup} + t_{F51,ik,pri} \leq 2 * \mathrm{CTI}^{\max} \quad (3)$$

- For the backward direction of fault current to the relay R_i:

$$2 * \mathrm{CTI}^{\min} \leq t_{F51,(backward-backward-i)k,backup} + t_{F51,(backward-i)k,backup} + t_{F51,ik,pri} \leq 2 * \mathrm{CTI}^{\max} \quad (4)$$

where CTI is a coordination time interval between two adjacent relays, commonly $\mathrm{CTI} \in \left\{\mathrm{CTI}^{\min}, \mathrm{CTI}^{\max}\right\} = \{0.2, 0.5\}$ [57,58]; $t_{F51,ik,pri}$ is the operation time of the i-th relay R_i when it works as primary protection for a k faulted location in the protected line/zone; $t_{F51,(upward-i)k,backup}$ is the backup operating time of the upward adjacent relay of the relay R_i; $t_{F51,(upward-upward-i)k,backup}$ is the backup operating time of the last upward adjacent relay of the relay R_i in the OCR triple; $t_{F51,(backward-i)k,backup}$ is the backup operating time of the backward adjacent relay of the relay R_i; and $t_{F51,(backward-backward-i)k,backup}$ is the backup operating time of the last backward adjacent relay of the relay R_i in the OCR triple.

In general, the optimization of the objective function is subjected to the following constraint conditions, (i) relay characteristic constraints; and (ii) protection coordination constraints. The former contains the relay operating time, TDS multiplier, coefficients of the inverse-time curve, and the pick-up current of OC relays. The latter considers the operation time difference of each pair of primary and backup OCRs as well as the total tripping time of each OCR triple.

2.3. Coordination Constraints of OCRs

2.3.1. Coordination Time Interval

According to IEEE 242-2001 standards, a CTI between primary and backup OCRs is usually selected in a range of 0.2 s to 0.5 s [57,58]. The CTI considers main factors such as the operating time of CBs, current transformer (CT) errors, the signal sending time of OCRs, and a safety margin [75]. If the primary relay fails to clear a fault given at the location k, then the backup relay will be activated to send the tripping signals to the related CBs after a certain CTI plus the failed operating time of the primary relay. The operating time T_{F51_jk} of the j-th backup relay (R_j) for a k faulted location in the network is expressed by Equation (5).

$$T_{F51\_jk} - T_{F51\_ik} \geq \text{CTI} \tag{5}$$

where T_{F51_jk} is calculated by Equation (6) as follows.

$$T_{F51\_jk} = TDS_j \left[\frac{A}{\left(I_{f\_jk} / I_{pu\_j} \right)^B - 1} + C \right] \tag{6}$$

where TDS_j and I_{pu_j} are the time-dial setting and pick-up current parameters of the j-th back-up relay, respectively; and I_{f_jk} is the fault current seen by the j-th back-up relay (R_j) regarding a k fault location in the distribution network. It is noted that all OC relays on a feeder of distribution network will have the same pick-up current threshold I_{pu}. The selection of pick-up current threshold for the OC relays is specifically presented in Section 2.3.4.

2.3.2. Boundary on Relay Operating Time

The operating time of OC relays has a practical boundary by two limits, $T_{ik}^{\min}$ and $T_{ik}^{\max}$, which can be formulated as the following:

$$T_{ik}^{\min} \leq T_{ik} \leq T_{ik}^{\max}, \forall i = 1, 2, \ldots n \tag{7}$$

where $T_{ik}^{\min}$ and $T_{ik}^{\max}$ are the minimum and maximum operation times of the i-th relay R_i when it operates as primary protection for a faulted location k in the DN, respectively. The value of $T_{ik}^{\min}$ depends on relay manufacturers, usually being higher than 0.01 s, while $T_{ik}^{\max}$ is the critical fault clearing time to avoid the damage of equipment as well as maintain the stability of power system, usually being lower than one second [32,33].

The Time-Dial Setting (TDS) is bounded by an available range of settings supplied by the relay manufacturer, which can be expressed as follows:

$$TDS_i^{\min} \leq TDS_i \leq TDS_i^{\max}, \forall i = 1, 2, \ldots n \tag{8}$$

where $TDS_i^{\min}$ and $TDS_i^{\max}$ are the minimum and maximum TDS values of the i-th relay R_i, respectively. The minimum and maximum available TDS values are usually in a range of 0.025 to 1.2 [32,33]. This study selects an available range of 0.01 to 3.2, respectively, for $TDS_i^{\min}$ and $TDS_i^{\max}$.

Similarly, the boundary of A, B, and C coefficients of inverse-time protection curve can be formulated by:

$$\begin{cases} A_i^{\min} \leq A_i \leq A_i^{\max} \\ B_i^{\min} \leq B_i \leq B_i^{\max}, \forall i = 1, 2, \ldots n \\ C_i^{\min} \leq C_i \leq C_i^{\max} \end{cases} \tag{9}$$

where $A_i^{\min}$ and $A_i^{\max}$ are 0.009 and 150, respectively; $B_i^{\min}$ and $B_i^{\max}$ are 0.02 and 2.5, respectively; $C_i^{\min}$ and $C_i^{\max}$ are zero and 1.5, respectively, in this study. The number of intervals in a pre-determined range of A_i, B_i, and C_i is 50.

2.3.3. Calculating the Min-Max Confidence Interval of Fault Currents in the DN Having DGs

To increase the reliability of fault-current calculation results in the DN having DGs, this section will present a novel statistical data-filtering method to determine a min-max confidence interval of load power $[P_{load\_min}, P_{load\_max}]$ and load current $[I_{load\_min}, I_{load\_max}]$ at each load bus in the DN, as seen in Sections of Forecasting a Min-Max Confidence Interval of Load Power at Each Load Bus and Calculating a Min-Max Confidence Interval of Load Current at Each Load Bus, respectively. Next, a current-injection-based power-flow (CIBPF) analysis method is used to calculate the min-max confidence interval of bus voltage at any i-th bus on the DN,$[V_{i\_min}, V_{i\_max}]$, instead of using either nominal bus-voltage values or voltage values calculated right after some pre-determined cycles from the power-flow analysis, as referred to Section of The Current-Injection-Based Power Flow Analysis. Based on the confidence intervals of bus-voltages in the distribution network, an adaptable fault analysis technique depicted in Section of An Adaptable Fault Analysis Technique is proposed to calculate the min-max confidence intervals of fault currents contributed by different DG units and fault current contributed by the utility which are used for effectively selecting tripping and pick-up thresholds of definite-time and inverse-time OC functions in the same OCR. In general, this adaptable fault analysis method contains four main steps: (i) forecasting a min-max confidence interval of load power at each load bus on a feeder of distribution network [81,82]; (ii) calculating a min-max confidence interval of load current at each load bus on the feeder; (iii) doing the current-injection-based power flow analysis to find a min-max confidence interval of voltage at each bus where has already installed the OC relay; and (iv) performing an adaptable fault analysis method to determine a min-max confidence interval of fault currents for each fault type in the DG-contained distribution network.

(i) Forecasting a Min-Max Confidence Interval of Load Power at Each Load Bus

Figure 2 shows a flow diagram of forecasting a min-max confidence interval of load power at each load bus in the DN. According to the work [82], there are seven main steps to forecast a min-max confidence interval of load power at each load bus on a feeder of distribution network as the following.

- Step 1—Input the historical load profiles at each load bus and perform the wrangling of the input data.
- Step 2—Calculate Probability Density Function (PDF) of load data and check whether the load data are in a Gaussian distribution or not. If the input load data have a Gaussian distribution, it is continued to Step 6.
- Step 3—If the input load data are not normally distributed, then the "differencing" method is used to eliminate the data trend by creating a new differential load data series in the one-day-ahead basis and the PDF of new differential load data series will be next calculated. When its PDF is in a Gaussian distribution, Step 6 will be implemented.
- Step 4—If the new differential data series is still not normally distributed, a Principal Components Analysis (PCA) method is conducted; and then the PDF is re-calculated for new differential load sub-datasets. If the new differential load sub-datasets are normally distributed, then it is continued with Step 6; otherwise, it goes to Step 5.
- Step 5—A 'dendrogram' method is conducted over the whole new differential load data series to explore the relationship among 15-min, 30-min, or hourly load data points, and then cluster them into many smaller differential load sub-datasets. Subsequently, it will go to Step 6.
- Step 6—The input load data at Step 2, the new differential load data series at Step 3, the new differential load sub-datasets at Step 4, or the smaller differential load sub-datasets at Step 5 are filtered-out with a possible confidence range of 13 levels, specifically from 90% to 99% with an increasing interval of 1%, 4.5-sigma (~99.73%), 5.5-sigma (~99.9937%), and 6-sigma (~99.99966%). Then, it is shown that the best con-

fidence interval of load data will be determined by an artificial neural network (ANN) forecasting model with the lowest Mean Absolute Percentage Error (MAPE) metric.

- Step 7—Applying the best confidence interval at Step 6 to eliminate unexpected outliers/noises of the original input load data; and then a min-max confidence interval of load power, $[P_{load\_min}, P_{load\_max}]$, at each load bus will be calculated by Equation (10).

$$\begin{cases} P_{\text{load\_max}} = \mu_P + \frac{Z}{\sqrt{N}}\sigma_P \\ P_{\text{load\_min}} = \mu_P - \frac{Z}{\sqrt{N}}\sigma_P \end{cases} \quad (10)$$

where a Z factor is taken from a normal/Gaussian distribution table corresponding to the best confidence level; μ_P is the mean value of load power at each load bus; N is the number of observed load data points; and σ_P is the standard deviation of the analyzed load data.

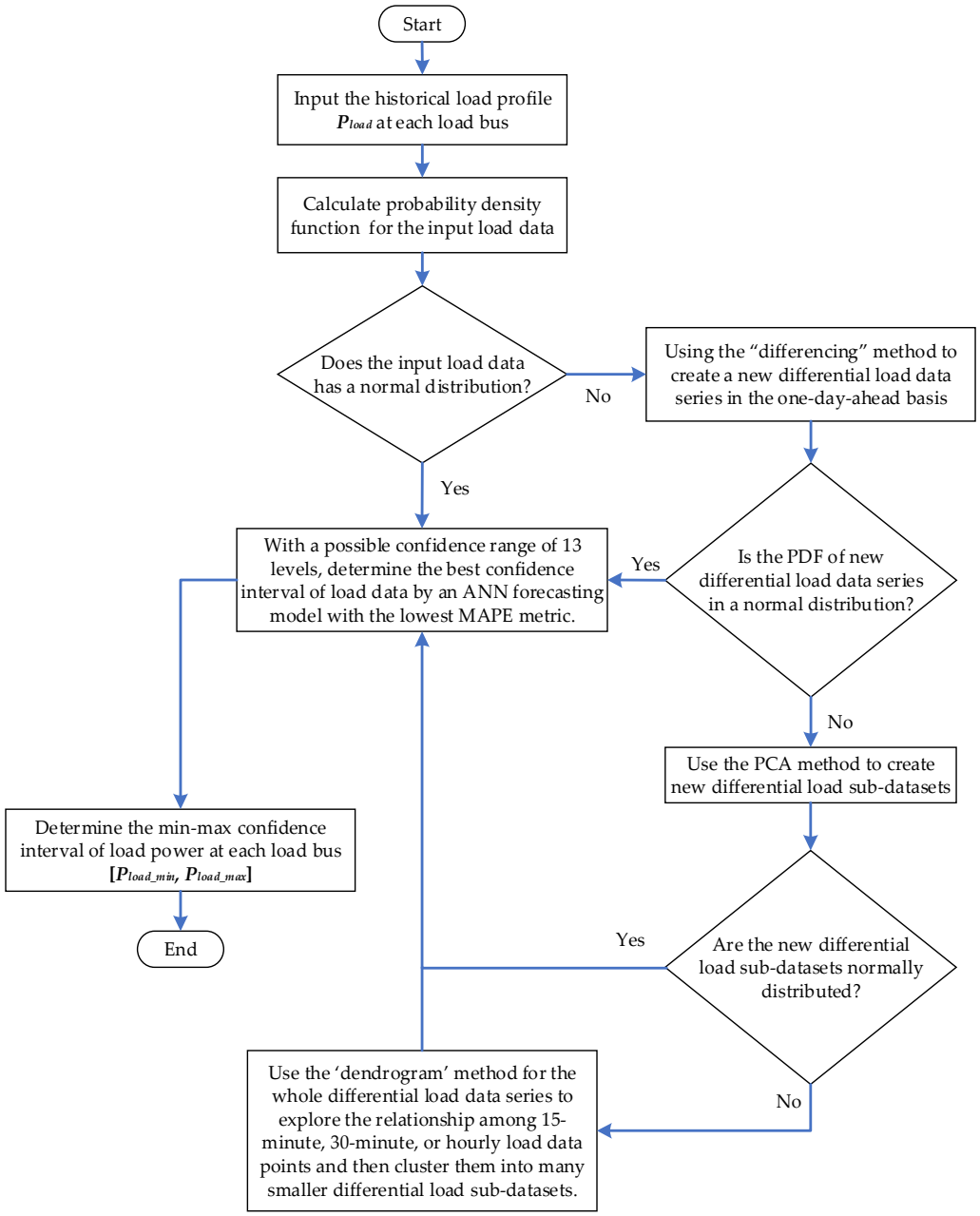

Figure 2. A flow diagram of forecasting a min-max confidence interval of load power at each load bus in the DN.

(ii) Calculating a Min-Max Confidence Interval of Load Current at Each Load Bus

Based on the min-max confidence interval of load power at each load bus in the DN and the nominal bus-voltage value, a min-max confidence interval of load current $[I_{\text{load\_min}}, I_{\text{load\_max}}]$ at each load bus can be calculated by:

$$\begin{cases} I_{\text{load\_min}} = \frac{P_{\text{load\_min}}}{V_{\text{nom}}} \\ I_{\text{load\_max}} = \frac{P_{\text{load\_max}}}{V_{\text{nom}}} \end{cases} \tag{11}$$

where V_{nom} is the nominal bus-voltage value. The minimum and maximum load current values, $I_{\text{load\_min}}$ and $I_{\text{load\_max}}$, at each bus are used for the current injection-based power flow analysis in the distribution network with DGs.

(iii) The Current-Injection-Based Power Flow Analysis

After the min-max confidence thresholds of load current at each load bus have been appropriately determined, they will be used for calculating voltage-fluctuating thresholds at all buses of the DG-based distribution network through the current-injection-based power-flow (CIBPF) analysis [83–86]. Then, the calculated voltage-fluctuating thresholds will be input to an adaptable fault analysis technique as mentioned in Section of An Adaptable Fault Analysis Technique. The modified (CIBPF) analysis method uses two matrices which are (i) branch currents (BC) matrix and (ii) bus voltages (BV) matrix. By considering the i-th bus in the distribution network, the power injected into this i-th bus can be expressed by Equation (12).

$$S_i = (P_i + jQ_i) = (P_{G,i} - P_{L,i}) + j(Q_{G,i} - Q_{L,i}), \forall i = 1, 2, \ldots, N \tag{12}$$

where $P_{G,i}$ and $Q_{G,i}$ are the active and reactive power of a generation source at the i-th bus, respectively; and $P_{L,i}$ and $Q_{L,i}$ are the active and reactive power of a load connected to the i-th bus, respectively. It is noted that a distribution network is assumed to have N buses.

The injection of equivalent current to the i-th bus at the k-th iteration of the power flow analysis is calculated by Equation (13) as below:

$$I_i^k = I_i^{real}\left(V_i^k\right) + jI_i^{imag}\left(V_i^k\right) = \left(\frac{P_i + jQ_i}{V_i^k}\right)^*, \forall i = 1, 2, \ldots, N \tag{13}$$

where V_i^k and I_i^k are the bus voltage and the equivalent current injected to the i-th bus at the k-th iteration, respectively; I_i^{real} and I_i^{imag} are real and imaginary components of the equivalent current injected to the i-th bus, which are considered as a function of V_i^k.

By considering a DG-integrated distribution network as in Figure 3, the injected-to-bus power can be properly converted to the injected-to-bus current by conducting Equation (13). According to [84,86], the relationship between the $[BC]$ matrix and the $[BV]$ matrix can be obtained through Kirchhoff laws. The [BC] matrix is determined by the injected-to-bus currents, as shown in Equation (14).

$$\begin{bmatrix} B_1 \\ B_2 \\ B_3 \\ B_4 \\ B_5 \end{bmatrix} = \begin{bmatrix} 1\,1\,1\,1\,1 \\ 0\,1\,1\,1\,1 \\ 0\,0\,1\,1\,0 \\ 0\,0\,0\,1\,0 \\ 0\,0\,0\,0\,1 \end{bmatrix} \begin{bmatrix} I_2 \\ I_3 \\ I_4 \\ I_5 \\ I_6 \end{bmatrix} \tag{14}$$

$$\begin{cases} I_6 = I_{load6} - I_{DG2} \\ I_5 = I_{load5} - I_{DG1} \\ I_4 = I_{load4} \\ I_3 = I_{load3} \\ I_2 = I_{load2} \end{cases} \tag{15}$$

$$I_{load\_l} \in \left\{ \frac{P_{load\_l\_\min}}{V_{nom}}; \frac{P_{load\_l\_\max}}{V_{nom}} \right\};\ l = 1 \ldots N_{load} \tag{16}$$

$$I_{DG\_d} = \left(\frac{P_{DG\_d} + jQ_{DG\_d}}{V_i} \right)^*;\ d = 1 \ldots N_{DG} \tag{17}$$

which B_1, B_2, B_3, B_4 and B_5 are the branch currents on the distribution network; I_2, I_3, I_4, I_5 and I_6 are the equivalent currents injected into the bus; I_{load_l} is the load current at a l-th load bus on the DN, with $l = 1, \ldots, N_{load}$; N_{load} is the total number of load buses; I_{DG_d} is the source current of the d-th DG injected to the bus, with $d = 1, \ldots, N_{DG}$; N_{DG} is the total number of distributed generators penetrated to the DN; $P_{load\_l\_min}$ and $P_{load\_l\_max}$ are the minimum and maximum thresholds of load power at the l-th load bus, respectively, as calculated in Section of Forecasting a Min-Max Confidence Interval of Load Power at Each Load Bus; V_{nom} is the nominal bus-voltage value of the distribution network; P_{DG_d} and Q_{DG_d} represent the active and reactive power of the d-th DG, respectively; and V_i is the i-th bus voltage on the distribution system.

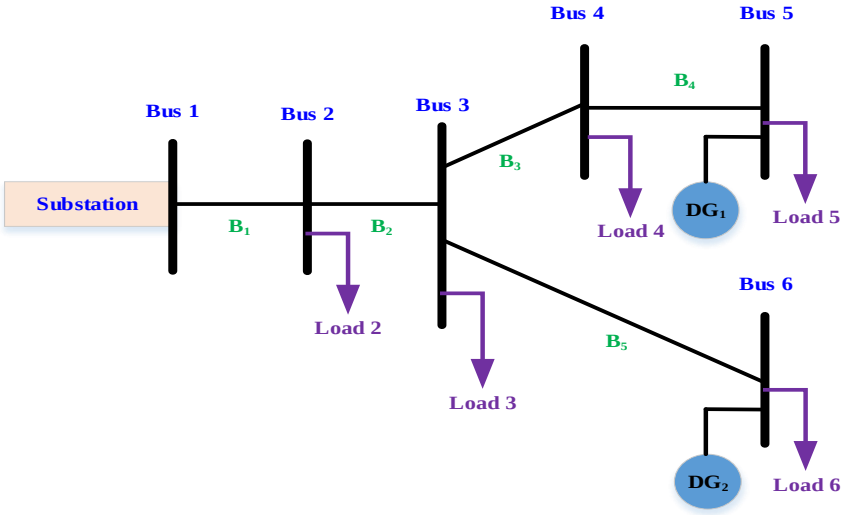

(**a**) A distribution system contains six buses and two DGs

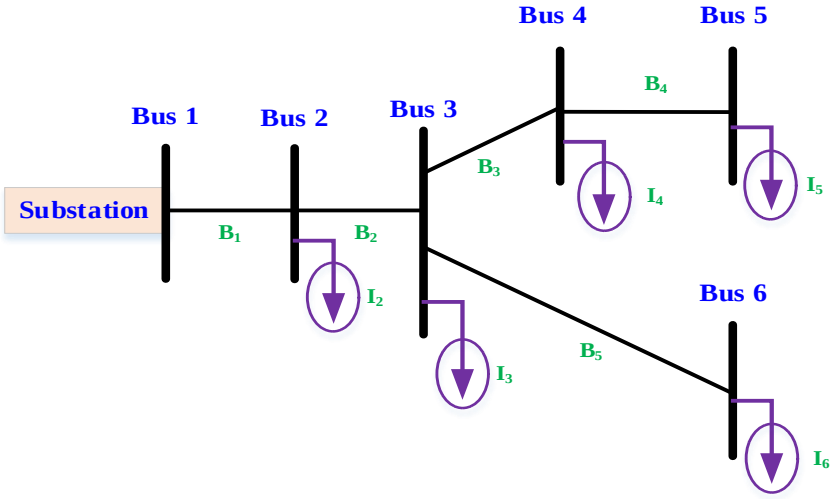

(**b**) The equivalent currents are injected into the buses on a single-line diagram of DN

Figure 3. A typical single-line diagram of DN with the integration of distributed generators.

In general, Equation (14) can be re-written as the following:

$$[BC] = [C][I] \tag{18}$$

where a [*C*] matrix is an upper triangular matrix filled by "0" or "1".

Next, the relationship of branch-currents matrix [*BC*] and bus-voltages matrix [*BV*] is shown in Equation (19):

$$[\Delta V] = [BV] = \begin{bmatrix} V_1 \\ V_1 \\ V_1 \\ V_1 \\ V_1 \end{bmatrix} - \begin{bmatrix} V_2 \\ V_3 \\ V_4 \\ V_5 \\ V_6 \end{bmatrix} = \begin{bmatrix} Z_{12} & 0 & 0 & 0 & 0 \\ Z_{12} & Z_{23} & 0 & 0 & 0 \\ Z_{12} & Z_{23} & Z_{34} & 0 & 0 \\ Z_{12} & Z_{23} & Z_{34} & Z_{45} & 0 \\ Z_{12} & Z_{23} & 0 & 0 & Z_{36} \end{bmatrix} \begin{bmatrix} B_1 \\ B_2 \\ B_3 \\ B_4 \\ B_5 \end{bmatrix} \tag{19}$$

$$V_j = V_i - B_i Z_{ij} \rightarrow B_i Z_{ij} = V_i - V_j, \ \forall i, j = 1, 2, \ldots, N; \ i \neq j \tag{20}$$

which V_i is the *i*-th bus voltage; V_j is the *j*-th bus-voltage; and Z_{ij} is the line impedance between bus *i* and bus *j*. Equation (19) can be generally re-written as follows.

$$[\Delta V] = [BV] = [Z][BC] \tag{21}$$

where $[\Delta V]$, or called $[BV]$, is the matrix of voltage drop between the bus *i* and the bus *j* on the DN; and [*Z*] is a lower triangular matrix of line impedances in the system.

In summary, when the min-max confidence interval of load power at the *l*-th load bus, $[P_{load\_l\_min}, P_{load\_l\_max}]$, has been already calculated/forecasted, the min-max confidence interval of load current, $[I_{load\_l\_min}, I_{load\_l\_max}]$, will be then appropriately determined. Next, the min-max confidence interval of equivalent current injected into the *i*-th bus, is also promptly defined. After that, the $[BC_{min}]$ and $[BC_{max}]$ matrices are calculated by Equation (18), with $[BC_{min}] = [B_{1\_min} B_{2\_min} \ \ldots \ B_{i\_min}]^T$ and $[BC_{max}] = [B_{1\_max} B_{2\_max} \ \ldots \ B_{i\_max}]^T$. Finally, the $[\Delta V_{min}]$ and $[\Delta V_{max}]$ voltage-drop matrices will be determined by Equation (21). As a result, the min-max confidence interval of bus voltage at any *i*-th bus on the DN, $[V_{i\_min}, V_{i\_max}]$, can be effectively calculated, specifically for $[V_1] - [B_{i\_min}] = [V_{i\_max}]$ and $[V_1] - [B_{i\_max}] = [V_{i\_min}]$ in this study. It is worth noting that V_1 is the nominal voltage value of bus 1 (also called the slack bus) in the distribution network.

- Solving the power flow problem in case of a radial distribution network

  To obtain the $[\Delta V]$ matrix, Equation (18) is substituted to Equation (21) as the following:

$$[\Delta V] = [Z][C][I] = [PF][I] \tag{22}$$

The $[PF]$ matrix in Equation (22) can be determined by a Lower-Upper (LU) factorization solution. The $[PF]$ matrix can be factorized by two $[Z]$ and $[C]$ matrices, where $[C]$ is the upper triangular matrix and $[Z]$ is the lower triangular matrix. The use of LU-decomposition and forward/backward algorithms allows skipping the calculation of Jacobian matrices or admittance matrices. Therefore, the computation time of power flows can be significantly reduced. As a result, the LU-decomposition-based power-flow analysis can be adaptable to the online power-flow analysis for a DG-integrated distribution system, as referred to Equation (23).

$$\begin{cases} I_i^k = I_i^{real}\left(V_i^k\right) + jI_i^{imag}\left(V_i^k\right) = \left(\frac{P_i + jQ_i}{V_i^k}\right)^* \\ \left[\Delta V_i^{k+1}\right] = [PF]\left[I_i^k\right] \\ [PF] = [Z][C] \\ \left[V_i^{k+1}\right] = [V_1] - \left[\Delta V_i^{k+1}\right] \end{cases} \tag{23}$$

where *k* is the iteration number of the current-injection-based power-flow analysis method.

- Solving the power flow problem in case of a ring-type distribution network

Figure 4 shows a single-line diagram of meshed distribution network. A new branch is connected from bus 5 to bus 6, hence, the equivalent currents at all buses are calculated as the following. Equation (19) can be re-formulated by:

$$[\Delta V] = [BV] = \begin{bmatrix} V_1 \\ V_1 \\ V_1 \\ V_1 \\ V_1 \\ 0 \end{bmatrix} - \begin{bmatrix} V_2 \\ V_3 \\ V_4 \\ V_5 \\ V_6 \\ 0 \end{bmatrix} = \begin{bmatrix} Z_{12} & 0 & 0 & 0 & 0 & 0 \\ Z_{12} & Z_{23} & 0 & 0 & 0 & 0 \\ Z_{12} & Z_{23} & Z_{34} & 0 & 0 & 0 \\ Z_{12} & Z_{23} & Z_{34} & Z_{45} & 0 & 0 \\ Z_{12} & Z_{23} & 0 & 0 & Z_{36} & 0 \\ 0 & 0 & Z_{34} & Z_{45} & -Z_{36} & Z_{56} \end{bmatrix} \begin{bmatrix} B_1 \\ B_2 \\ B_3 \\ B_4 \\ B_5 \\ B_6 \end{bmatrix} \tag{24}$$

$$\begin{bmatrix} \Delta V \\ 0 \end{bmatrix} = [Z_{new}] \begin{bmatrix} BC \\ B_{new} \end{bmatrix} \tag{25}$$

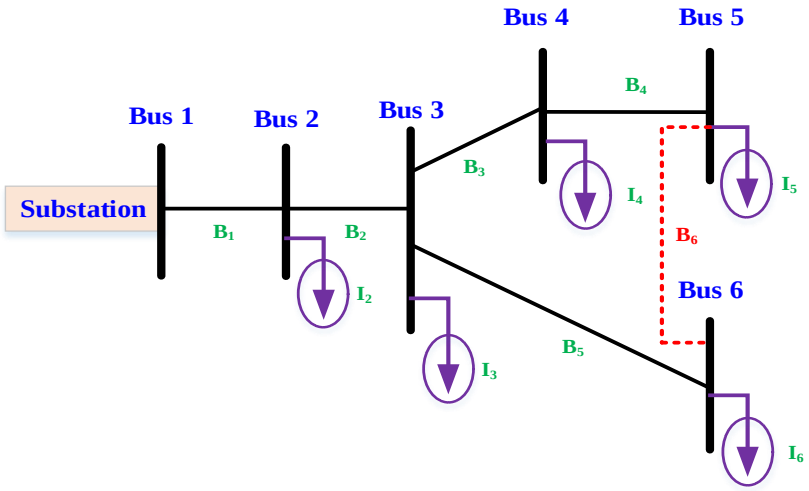

Figure 4. A typical single-line diagram of meshed distribution network.

Generally, a new branch B_k is built on a distribution network to create a ring topology; specifically, the new branch is connected from the bus i to the bus j. The initial [Z] matrix can be re-calculated by the following steps: (i) adding a new row to the initial [Z] matrix and each element of the added new row is calculated by subtracting the j-th row from the i-th row; (ii) an element of the new row that belongs to a diagonal of [Z] matrix is also an intersectional position of the new row and the new column of the [Z] matrix; and it will be an impedance of the new branch B_k.

In addition, Equation (14) is also re-written as follows:

$$\begin{bmatrix} B_1 \\ B_2 \\ B_3 \\ B_4 \\ B_5 \\ B_6 \end{bmatrix} = \begin{bmatrix} 1 & 1 & 1 & 1 & 1 & 0 \\ 0 & 1 & 1 & 1 & 1 & 0 \\ 0 & 0 & 1 & 1 & 0 & 1 \\ 0 & 0 & 0 & 1 & 0 & 1 \\ 0 & 0 & 0 & 0 & 1 & -1 \\ 0 & 0 & 0 & 0 & 0 & 1 \end{bmatrix} \begin{bmatrix} I_2 \\ I_3 \\ I_4 \\ I_5 \\ I_6 \\ B_6 \end{bmatrix} \tag{26}$$

$$\begin{bmatrix} BC \\ B_{new} \end{bmatrix} = [C_{new}] \begin{bmatrix} I \\ B_{new} \end{bmatrix} \tag{27}$$

A new branch B_k is built in a meshed distribution network, which is connected from the bus i to the bus j. The [C] matrix is then re-calculated by the following steps: (i) copying the elements of the column related to the i-th bus to the k-th column (called a new column) and subtracting the elements of the column related to the j-th bus from this new column; and (ii) adding the value (+1) to the k-th row and k-th column in the [C] matrix.

Substituting two Equations (27) and (25) into Equation (22), it shows that:

$$\begin{bmatrix} \Delta V_{new} \\ 0 \end{bmatrix} = [Z_{new}][C_{new}] \begin{bmatrix} I \\ B_{new} \end{bmatrix} = \begin{bmatrix} AM^T \\ MN \end{bmatrix} \begin{bmatrix} I \\ B_{new} \end{bmatrix} \quad (28)$$

Then, the Kron reduction method is applied to Equation (28), it becomes:

$$[\Delta V_{new}] = \left[A - M^T N^{-1} M\right][I] = [PF_{new}][I] \quad (29)$$

As a result, Equation (29) with the $[PF_{new}]$ matrix can be solved by the LU factorization method as mentioned in Equation (23).

(iv) An Adaptable Fault Analysis Technique

According to the work in [6], a simplified and automated fault-current calculation approach can be appropriately modified for this study. The total short-circuit current observed by the *r*-th OCR for a faulted location in the DG-contained DN is calculated by Equation (30). The configuration of DG-based distribution network is changeable due to two plug-and-play and peer-to-peer characteristics of DGs, so a real-time management system (RTMS) using the SCADA function is deployed to observe the operating states of DGs as well as the working status of protective devices like OCRs and other devices such as CBs, tie switches, load break switches, or reclosers in the DN.

$$I_{f,r} = I_{f,grid-r} + \sum_{i=1}^{N_{DG}} \left(k_{ri} * I_{f,DGi} * T_{DGi}\right), \forall I_{f,r} \in \left(I_{f,r}^{\min}, I_{f,r}^{\max}\right) \quad (30)$$

where $I_{f,r}$ is the total short-circuit current observed by the *r*-th OCR for a faulted location in the DN; $I_{f,grid-r}$ is the grid fault-current component seen by the *r*-th OCR for the considered fault location; N_{DG} is the total number of IBDGs and RBDGs integrated to the DN; k_{ri} is a fault-current division coefficient of the *i*-th DG impacting the operation of the *r*-th OCR; $I_{f,DGi}$ is the fault current at terminals of the *i*-th DG; and T_{DGi} is the operating status of the *i*-th DG, specifically, $T_{DGi} = 1$ for the "on-grid" mode and $T_{DGi} = 0$ for the "off-grid" mode.

Generally, if a distribution system contains the N_{DG} total number of DGs and the M_{OCPR} total number of OCRs, the fault-current division coefficient of each DG unit impacting the operation of each OCR can be properly calculated by Equation (30). Symmetrical impedances are used for calculating the fault-current division coefficients of DGs and the grid sources impacting all OCRs in the DN. Due to the SCADA function of RTMS, the symmetrical impedance matrices can be continuously updated corresponding to different DN topologies as well as the operating status of DGs such that the fault-current division coefficients of DGs will be quickly determined. Equation (30) can be re-written by:

$$\begin{cases} I_{f,r}^{\min} = I_{f,grid-r}^{\min} + \sum_{i=1}^{N_{DG}} \left(k_{ri} * I_{f,DGi}^{\min} * T_{DGi}\right) \\ I_{f,r}^{\max} = I_{f,grid-r}^{\max} + \sum_{i=1}^{N_{DG}} \left(k_{ri} * I_{f,DGi}^{\max} * T_{DGi}\right) \end{cases} \quad (31)$$

where $I_{f,r}^{\min}$ and $I_{f,r}^{\max}$ are the min-max confidence thresholds of total short-circuit current observed by the *r*-th OCR for a faulted location in the DN; $I_{f,grid-r}^{\min}$ and $I_{f,grid-r}^{\max}$ are the min-max confidence thresholds of grid fault-current for a given fault location; $I_{f,DGi}^{\min}$ and $I_{f,DGi}^{\max}$ are the minimum and maximum fault-current values of the *i*-th IBDG/RBDG at their terminals which are pre-defined, specifically, 5 pu~10 pu for RDBGs [87,88] and 1.0~2.0 pu for IBDGs [89,90].

- Determining the min-max confidence thresholds of fault current from the grid

To calculate $I_{f,grid-r}^{\min}$ and $I_{f,grid-r}^{\max}$, the min-max confidence interval of bus voltages, $[V_{i\_\min}, V_{i\_\max}]$, must be determined as shown in Section of The Current-Injection-Based Power Flow Analysis. Then, the values $V_{i\_\min}$ and $V_{i\_\max}$ are respectively substituted to

$V_i(0)$ as depicted in Equation (32). It is assumed that the total number of OCRs is equal to that of buses in the DN, i.e., $M_{OCPR} = N$.

$$\begin{cases} \begin{bmatrix} V_{f,1,k} \\ \dots \\ V_{f,i,k} \\ \dots \\ V_{f,N,k} \end{bmatrix} = \begin{bmatrix} V_1 \\ \dots \\ V_i(0) \\ \dots \\ V_N(0) \end{bmatrix} - \left([Z_{\text{bus}}]_{N\times N} + \left[Z_{f,k} \right]_{N\times N} \right) \begin{bmatrix} I^{\min}_{f,grid-1,k} \\ \dots \\ I^{\min}_{f,grid-i,k} \\ \dots \\ I^{\min}_{f,grid-N,k} \end{bmatrix}, V_i(0) = V_{i\_\min}, \forall i \in N \\ \begin{bmatrix} V_{f,1,k} \\ \dots \\ V_{f,i,k} \\ \dots \\ V_{f,N,k} \end{bmatrix} = \begin{bmatrix} V_1 \\ \dots \\ V_i(0) \\ \dots \\ V_N(0) \end{bmatrix} - \left([Z_{\text{bus}}]_{N\times N} + \left[Z_{f,k} \right]_{N\times N} \right) \begin{bmatrix} I^{\max}_{f,grid-1,k} \\ \dots \\ I^{\max}_{f,grid-i,k} \\ \dots \\ I^{\max}_{f,grid-N,k} \end{bmatrix}, V_i(0) = V_{i\_\max}, \forall i \in N \end{cases} \quad (32)$$

where $V_{f,i,k}$ is the fault voltage of the i-th bus for a k faulted location in the DN; $V_i(0)$ is the min/max pre-fault bus-voltage at the i-th bus; the values $I^{\min}_{f,grid-r}$ and $I^{\max}_{f,grid-r}$ are equal the values $I^{\min}_{f,grid-i}$ and $I^{\max}_{f,grid-i}$, respectively, because each bus i has already installed the r-th OCR in the system; $[Z_{\text{bus}}]_{N\times N}$ is the Thevenin impedance matrix with a size of $N \times N$; and $\left[Z_{f,k} \right]_{N\times N}$ is the fault impedance at the k faulted location; normally, the faulted location is considered at the buses of a distribution system. For the asymmetrical faults, the positive- negative-, and zero-sequence Thevenin impedance matrices $\left[Z^{012}_{bus} \right]_{N\times N}$ need to be calculated. The subscripts 0, 1, 2 are represented as zero-, positive-, and negative-sequence components, respectively. Hence, Equation (32) can be re-written as the following.

$$\begin{cases} V^{012}_{f,i,k} = V^{012}_i(0) - \left(\left[Z^{012}_{bus} \right]_{N\times N} + \left[Z_{f,k} \right]_{N\times N} \right) \begin{bmatrix} I^{012,\min}_{f,grid-1,k} \\ \dots \\ I^{012,\min}_{f,grid-i,k} \\ \dots \\ I^{012,\min}_{f,grid-N,k} \end{bmatrix}, V^{012}_i(0) = V^{012}_{i\_\min}, \forall i \in N \\ V^{012}_{f,i,k} = V^{012}_i(0) - \left(\left[Z^{012}_{bus} \right]_{N\times N} + \left[Z_{f,k} \right]_{N\times N} \right) \begin{bmatrix} I^{012,\max}_{f,grid-1,k} \\ \dots \\ I^{012,\max}_{f,grid-i,k} \\ \dots \\ I^{012,\max}_{f,grid-N,k} \end{bmatrix}, V^{012}_i(0) = V^{012}_{i\_\max}, \forall i \in N \end{cases} \quad (33)$$

- Determining fault-current division coefficients of DGs in the DN

In general, the min-max confidence thresholds of grid fault current seen by the r-th relay for a given fault, $I^{\min}_{f,grid-r}$ and $I^{\max}_{f,grid-r}$, can be used as the basis for parameter settings of the r-th relay in the DN. A fault-current division coefficient of the i-th RBDG impacting the operation of the r-th relay is expressed by:

$$\begin{cases} k^{\min}_{ri} = \frac{I^{\min}_{f,DGi-r}}{I^{\max}_{f,DGi}} = \left(\frac{V_{i\_\min}}{Z_{ir}} \right) / I^{\max}_{f,DGi}, \forall i \neq r \\ k^{\max}_{ri} = \frac{I^{\max}_{f,DGi-r}}{I^{\min}_{f,DGi}} = \left(\frac{V_{i\_\max}}{Z_{ir}} \right) / I^{\min}_{f,DGi}, \forall i \neq r \\ k_{ri} = 1 \text{ for } i = r \end{cases} \quad (34)$$

where $k^{\min}_{ri}$ and $k^{\max}_{ri}$ are the minimum and maximum fault-current division coefficients of the i-th RBDG with respect to the r-th relay, respectively; it is assumed that the i-th RBDG is connected to the i-th bus in the DN, so Z_{ir} is the impedance from the bus i to the bus r that is determined from the $[Z_{\text{bus}}]_{N\times N}$ matrix. In the case of $i = r$, the k_{ri} coefficient is unit; and the value k_{ri} is in an available range of [0~1].

On the other hand, the fault-current division coefficient k_{ri} of the i-th IBDG impacting the operation of the r-th relay can be expressed by Equation (35):

$$\begin{cases} k_{i-downstream\_r} = \frac{Z_{i-upstream\_r}}{Z_{i-downstream\_r}+Z_{i-upstream\_r}} \\ k_{i-upstream\_r} = \frac{Z_{i-downstream\_r}}{Z_{i-downstream\_r}+Z_{i-upstream\_r}} \quad \text{for a ring topology} \\ k_{ri} = 1 \text{ for a radial topology} \end{cases} \tag{35}$$

where the subscripts '$downstream\_r$' and '$upstream\_r$' represent the fault current direction of the i-th IBDG flowing into the downstream and upstream sites of the r-th relay respectively, with regard to a given fault location in the DN. When a fault occurs in the distribution system, the IBDG will limit its fault current contribution and operate as a fault current source. Therefore, the coefficient k_{ri} equals to 1 for a radial topology of DN. For the ring-type/meshed DN, it is necessary to calculate the downstream and upstream fault-current division coefficients $k_{i-downstream\_r}$ and $k_{i-upstream\_r}$ of the i-th DG regarding to the r-th relay, as referred to Equation (35). The $k_{i-downstream\_r}$ coefficient is selected in case the r-th relay is used to detect the fault at its upstream direction, whereas the $k_{i-upstream\_r}$ coefficient is selected only if the r-th relay is designed to detect the fault at its downstream direction.

In general, a $[K]$ coefficient matrix can be determined to show the fault-current contribution of N_{DG} DGs to M_{OCPR} relays (noted that the number of OCRs equals to the number of buses in the DN) as expressed in Equation (36).

$$[K] = \begin{bmatrix} k_{11} & k_{1i} & k_{1N_{DG}} \\ \cdots & \cdots & \cdots \\ k_{r1} & k_{ri} & k_{rN_{DG}} \\ \cdots & \cdots & \cdots \\ k_{M_{OCPR}1} & k_{M_{OCPR}i} & k_{M_{OCPR}N_{DG}} \end{bmatrix} \text{ with } \begin{cases} i = 1 \ldots N_{DG} \\ r = 1 \ldots M_{OCPR} = 1 \ldots N \end{cases} \tag{36}$$

where the k_{ri} element of $[K]$ matrix can be k_{ri}^{min}, k_{ri}^{max}, 1, $k_{i-downstream-r}$, or $k_{i-upstream-r}$ according to the type of DGs (e.g., IBDG or RBDG), the location of DGs, the location of OCRs, and the topology of DN (e.g., radial topology or ring topology). In addition, the $[K]$ matrix can also be applied to the unbalanced faults in the distribution system.

2.3.4. Selection of Pick-Up Currents for OC Relays

The pick-up current I_{pu} of OCR should be selected to be higher than the maximum possible load current and lower than the minimum fault current with a reliable security margin. The measurement error of current transformers (CTs) should also be considered for the pick-up current selection. The boundary of pick-up current of the r-th OCR, $I_{pu,r}^{\min}$ and $I_{pu,r}^{\max}$, is determined as below:

$$\begin{cases} I_{pu,r}^{\min} = \left(OLF + K_L \frac{e_{CT\%}}{100}\right) \frac{I_{load,r}^{\max}}{CTR} \\ I_{pu,r}^{\max} = \left(\frac{1}{3} - K_{SC} \frac{e_{CT\%}}{100}\right) \frac{I_{f,r}^{\min}}{CTR} \\ I_{pu,r}^{selected} = \frac{I_{pu,r}^{\min} + I_{pu,r}^{\max}}{2} \end{cases} \tag{37}$$

where OLF is the overload factor selected to 1.15 [91]; K_L and K_{SC} are the security factors to be higher than 1; $e_{CT\%}$ is the measurement error of current transformers selected to 10%; $I_{load,r}^{\max}$ is the maximum load current seen by the r-th relay based on the power-flow analysis results in Section of The Current-Injection-Based Power Flow Analysis; CTR is the current transformer ratio; $I_{f,r}^{\min}$ is the minimum total fault current observed by the r-th relay (normally considering a phase-to-phase (ph-ph) fault located at a remote end of the protected line) as presented in Section of An Adaptable Fault Analysis Technique; a

1/3 factor in Equation (37) is referred by the references [92,93]. In this study, the selected pick-up current $I_{pu,r}^{selected}$ of the r-th OCR will be the average of $I_{pu,r}^{\min}$ and $I_{pu,r}^{\max}$.

2.3.5. Selection of Tripping Currents for the OC Relays

Table 1 shows the selection of tripping currents of the OCRs in the DG-based distribution network. The fault-current analysis is performed at the remote end of the protected zones/lines in the DN, with four main types including (i) three phase-to-ground (3ph-G) fault, (ii) double-phase to-ground (2ph-G) fault, (iii) phase-to-phase (ph-ph) fault and iv) single-phase to-ground (1ph-G) fault. As a novel contribution of the paper, the protection coordination of the OCRs including 50P, 50G, 5P, and 51G functions is established for the maximum fault-current value of each fault type.

Table 1. Fault-current selection for the 50 and 51 OC functions.

Different OC Functions	Selection of Fault/Tripping Currents, I_{f_rk}	Descriptions
50P: Definite-time phase OC protection function	$I_{f\_rk\_F50P} = I_{f,r,ph-ph}^{\max}$ with $r = 1 \ldots N$	k is a given fault location at the remote end of the protected line/zone; and $I_{f,r,ph-ph}^{\max}$ is the maximum ph-ph fault current.
51P: Inverse-time phase OC protection function	$I_{f\_rk\_F51P} = I_{f,r,ph-ph}^{\max}$ with $r = 1 \ldots N$	
50G: Definite-time ground OC protection function	$I_{f\_rk\_F50G} = \min\left(I_{f,r,3ph-G}^{\max}, I_{f,r,2ph-G}^{\max}, I_{f,r,1ph-G}^{\max}\right)$ with $r = 1 \ldots N$	$I_{f,r,3ph-G}^{\max}$, $I_{f,r,2ph-G}^{\max}$ and $I_{f,r,1ph-G}^{\max}$ are the maximum 3ph-G, 2ph-G, and 1ph-G fault currents for a given fault location, respectively.
51G: Inverse-time ground OC protection function	$I_{f\_rk\_F51G} = \min\left(I_{f,r,3ph-G}^{\max}, I_{f,r,2ph-G}^{\max}, I_{f,r,1ph-G}^{\max}\right)$ with $r = 1 \ldots N$	

2.3.6. Summary of the Proposed ASPC Approach for OCRs in a DG-Based Distribution Network

Figure 5 shows a flow-chart of the ASPC approach for OCRs in the DN with DGs. There are five basic steps as the following:

- Step 1: Input the maximum fault-current values detected by each OCR corresponding to four different fault types (e.g., ph-ph, 1ph-G, 2ph-G, and 3ph-G) that occurred at the remote end of the protective zones/lines.
- Step 2: Select the pick-up and tripping/fault currents for the OC relays and define the tripping time of 50P and 50G functions, as shown in Table 1.
- Step 3: Based on the objective function Z in Equation (2), determine A, B, and C factors and TDS multiplier of 51P and 51G functions in each OCR by using three meta-heuristic algorithms, GSA, hybrid PSO&GSA and GA.
- Step 4: Check the tripping time of 50P/G and 51P/G functions and the constraint conditions of CTI between the primary and backup relays for the OCR pairs and the OCR triples as referred to Equations (3)–(5).
- Step 5: Select the appropriate protection coordination results for OCRs which are satisfied with the constraint conditions; and update the setting parameters to the related OCRs in the DG-based DN.

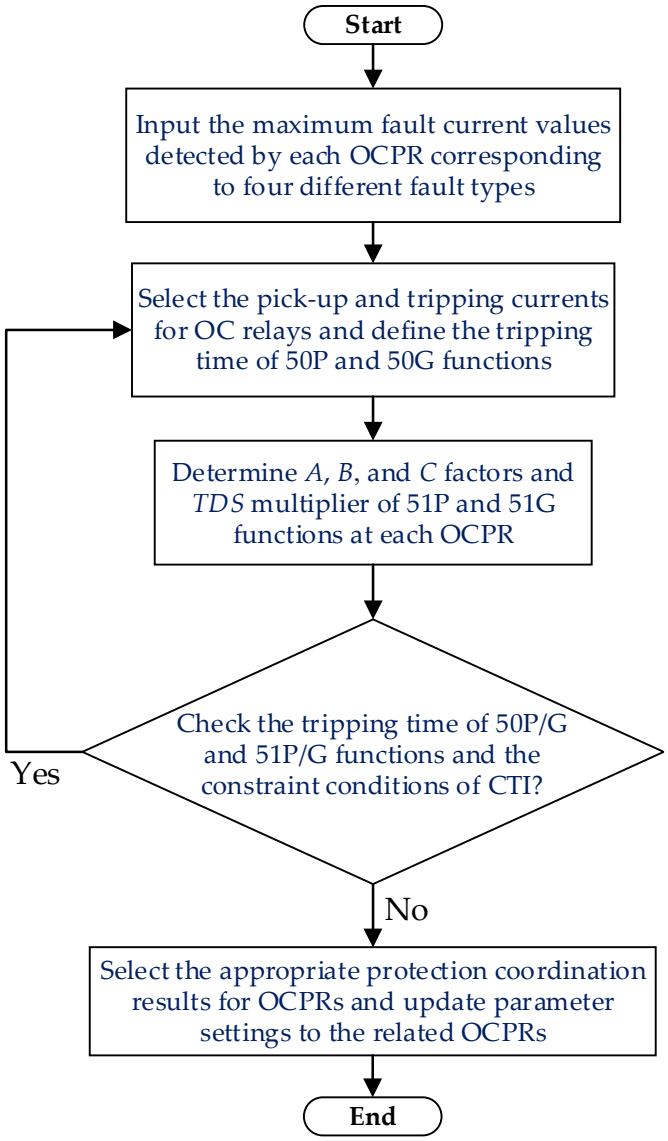

Figure 5. A general flow-chart of the proposed ASPC approach for OCRs in a DG-based distribution network.

2.4. Protection Coordination Algorithms

2.4.1. Gravitational Search Algorithm (GSA)

A Gravitational Search Algorithm (GSA) is based on the gravitational force and Newton's law of motion [94]. By considering a system with N agents (or N masses) with the d-th dimension in a certain search space, the gravitational force from the j-th agent to the i-th agent at the t-th time, $F_{ij}^{d}(t)$, can be expressed by Equation (38):

$$F_{ij}^{d}(t) = G(t)\frac{M_{pi}(t) \times M_{aj}(t)}{R_{ij}(t) + \in}\left(x_{j}^{d}(t) - x_{i}^{d}(t)\right) \tag{38}$$

where, $M_{aj}(t)$ is the active gravitational mass regarding to the j-th agent in the time t; $M_{pi}(t)$ is the passive gravitational mass regarding to the i-th agent; $\in$ is a small constant; $R_{ij}(t)$ represents the Euclidian distance between the agents i and j; x_{i}^{d} and x_{j}^{d} are the position of the i-th agent and the j-th agent at the d-th dimension, respectively; and $G(t)$ is a gravitational constant at the time t as referred to Equation (39).

$$G(t) = G_{0} \times \exp(-\alpha * {}^{iter}/_{\max\_iter}) \tag{39}$$

where G_0 and α are the initial value of gravitational constant and the descending coefficient, respectively, normally selected to 20 and 100; *'iter'* is the current number of iterations; and '*max_iter*' is the maximum number of iterations. In other words, $G(t)$ is a function of the initial value G_0 and is gradually decreased with respect to the time to control the search accuracy of the algorithm.

The Euclidian distance, $R_{ij}(t)$, between two agents i and j is calculated as the following.

$$R_{ij}(t) = \left|\left|X_i(t),\ X_j(t)\right|\right|_2 \tag{40}$$

where the position of the i-th agent and the j-th agent with n-dimensions, X_i and X_j, can be defined as below:

$$\begin{aligned} X_i &= \left(x_i^1, \ldots, x_i^d, \ldots, x_i^n\right), i = 1, 2, \ldots, N \\ X_j &= \left(x_j^1, \ldots, x_j^d, \ldots, x_j^n\right), j = 1, 2, \ldots, N \\ X &= \left\{X_1, \ldots, X_i \ldots, X_j, \ldots, X_N\right\} \end{aligned} \tag{41}$$

For the stochastic search algorithm, the total gravity force impacting the i-th agent at the d-th dimension, $F_i^d(t)$, is the sum of d-th components of the forces generated from other agents in a set of N agents with the random weighting factor $rand_j$ in an available interval [0, 1].

$$F_i^d(t) = \sum_{j=1, j\neq i}^{N} rand_j F_{ij}^d(t) \tag{42}$$

The acceleration of the i-th agent at the time t with the d-th dimension, $A_i^d(t)$, can be calculated by:

$$A_i^d(t) = \frac{F_i^d(t)}{M_{ii}(t)} \tag{43}$$

where $M_{ii}(t)$ is the inertial mass of the i-th agent at the time t.

For each iteration step, the velocity and position of the i-th agent are updated by the following equations.

$$Vel_i^d(t+1) = rand_i \times Vel_i^d(t) + A_i^d(t) \tag{44}$$

$$X_i^d(t+1) = X_i^d(t) + Vel_i^d(t+1) \tag{45}$$

where the next velocity of the i-th agent, $Vel_i^d(t+1)$, is the sum of a fraction of its current velocity $rand_i \times Vel_i^d(t)$ and its acceleration $A_i^d(t)$; '$rand_i$' is a random variable in the interval [0, 1]; and the next position of the i-th agent $X_i^d(t+1)$ is the sum of its current position, $X_i^d(t)$, and its next velocity, $Vel_i^d(t+1)$. It is noted that the use of a random variable is to give a randomized search characteristic of the algorithm.

The gravitational and inertia masses of the i-th agent can be calculated by the fitness evaluation which is referred to Equation (2) in Section 2.2. The greater mass is, the more efficient agent is. The better agents will have the higher attractive forces and the slower movement. The gravitational and inertia masses of the agent are assumed to be equal. The value of masses can be updated as follows.

$$M_{ai} = M_{pi} = M_{ii} = M_i,\ \forall i = 1, 2, \ldots, N \tag{46}$$

$$m_i(t) = \frac{fit_i(t) - worst(t)}{best(t) - worst(t)} \tag{47}$$

$$M_i(t) = \frac{m_i(t)}{\sum_{j=1}^{N} m_j(t)} \tag{48}$$

where $fit_i(t)$ is the fitness value of the i-th agent at the time t; $best(t)$ is the optimal solution, whereas $worst(t)$ is the worst solution of the algorithm. The $best(t)$ and $worst(t)$ parameters can be determined depending on two following problems.

- For the minimization value problem:

$$best(t) = \min\{fit_j(t)\}_{j\in\{1,\ldots,N\}} \quad (49)$$

$$worst(t) = \max\{fit_j(t)\}_{j\in\{1,\ldots,N\}} \quad (50)$$

- For the maximization value problem:

$$best(t) = \max\{fit_j(t)\}_{j\in\{1,\ldots,N\}} \quad (51)$$

$$worst(t) = \min\{fit_j(t)\}_{j\in\{1,\ldots,N\}} \quad (52)$$

All the procedures are involved in the GSA to find the optimal parameters of the OCRs referred to Figure 6.

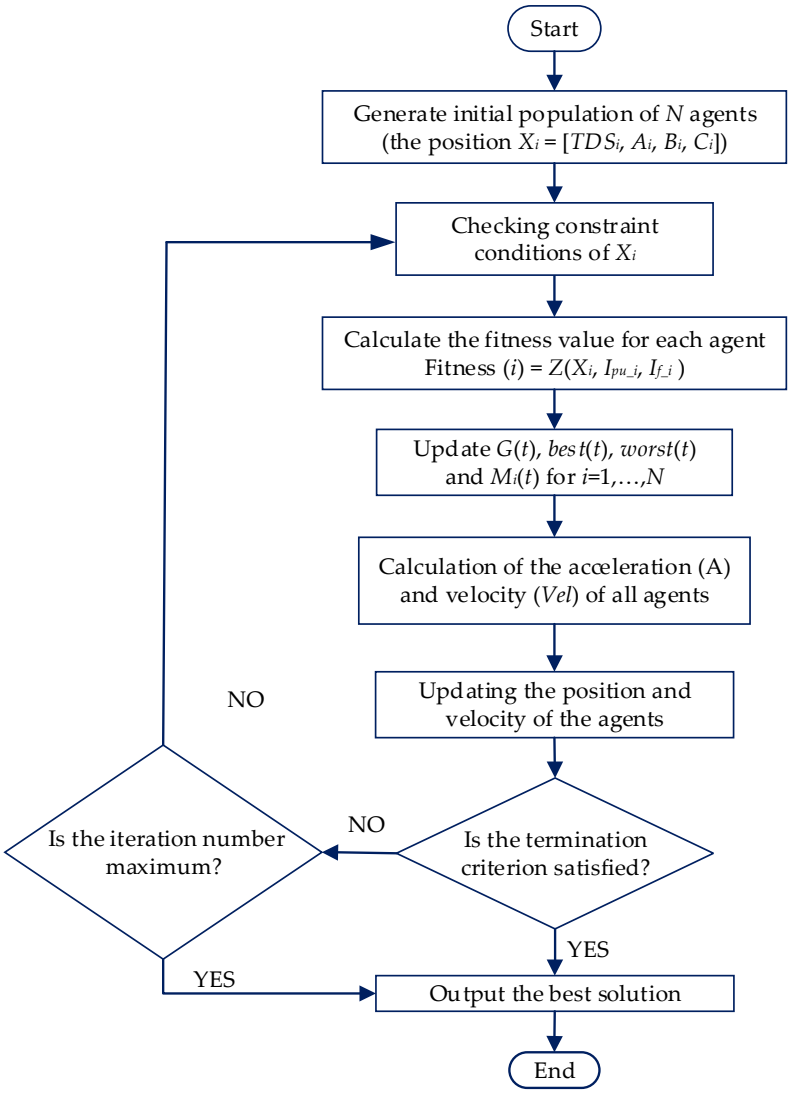

Figure 6. A flow chart of GSA applied to the ASPC approach of OCRs.

2.4.2. Hybrid Particle Swarm Optimization and Gravitational Search Algorithm (Hybrid PSO&GSA)

In the particle swarm optimization algorithm, the feasible solutions are called the particles/agents that fly in the d-dimensions search space by following the current optimal particles [95]. Let s_i and v_i denote the position and velocity of the i-th particle, respectively;

at each iteration, the velocity of each particle is updated by using its current position, velocity and its distance from the *pbest* to the *gbest* as shown in Equation (53).

$$\begin{aligned}
&v_{i,d}^{k+1} = \omega * v_{i,d}^{k} + C_1 * rand() * \frac{\left(pbest^k{}_i - s_{i,d}^k\right)}{\Delta t} + C_2 * rand() * \frac{\left(gbest^k - s_{i,d}^k\right)}{\Delta t} \\
&v_{i,d}^{k} \in [-v_{\max}, v_{\max}], v_{\max} = k s_{\max}, 0.1 \le k \le 1 \\
&s_{i,d}^{k} \in [-s_{\max}, s_{\max}] \\
&v_i^k = \left(v_{i,1}^k, v_{i,2}^k, \ldots, v_{i,d}^k\right) \\
&s_i^k = \left(s_{i,1}^k, s_{i,2}^k, \ldots, s_{i,d}^k\right) \\
&pbest^k{}_i = \left(pbest^k{}_{i,1} pbest^k{}_{i,2}, \ldots, pbest^k{}_{i,d}\right) \\
&gbest^k = \left(pbest^k{}_1, pbest^k{}_2, \ldots, pbest^k{}_N\right)
\end{aligned} \tag{53}$$

where $v_{i,d}^k$ is the current velocity of the i-th particle at the k-the iteration with the d-th dimension; $rand()$ is a random variable in the interval [0, 1]; $s_{i,d}^k$ is the current position of the i-th particle at the k-the iteration; C_1 and C_2 are the acceleration coefficients; $pbest^k{}_i$ is the personal best position of the i-th particle in the d-dimensions; $gbest^k$ is the global best position of all the particles in the d-dimensions; and Δt is the time step of the algorithm. Moreover, the weighting function ω can be expressed by Equation (54).

$$\omega = \omega_{\max} - \left(\frac{\omega_{\max} - \omega_{\min}}{iter_{\max}}\right) * iter \tag{54}$$

where $\omega_{\max}$ and $\omega_{\min}$ are the maximum and minimum weighting values, respectively, which are constant; *iter* is the current iteration number; and $iter_{\max}$ is the maximum number of iterations. The algorithm starts with the $\omega_{\max}$ value and decreases to the $\omega_{\min}$ value when the number of iterations increases.

In addition, each particle can update its position at the next time step (iteration) by using its current velocity to explore the search space for a better solution as follows:

$$s_{i,d}^{k+1} = s_{i,d}^k + v_{i,d}^{k+1} * \Delta t \tag{55}$$

where Δt is commonly set to one in this study. For the minimization value problem, the personal best position, *pbest*, is updated after the k-th iteration according to Equation (56).

$$pbest^{k+1}{}_i = \begin{cases} pbest^k{}_i & \text{if} \quad f\left(s_i^{k+1}\right) \ge f\left(pbest^k{}_i\right) \\ s_i^{k+1} & \text{if} \quad f\left(s_i^{k+1}\right) < f\left(pbest^k{}_i\right) \end{cases} \tag{56}$$

where f is the fitness/objective function which is referred to Equation (2) in Section 2.2.

The agents in the GSA do not share the population information with each other agent, so the PSO algorithm can be integrated with the GSA to improve the global optimal searching capability. In other words, the GSA is to use for the local searching ability while the PSO algorithm is to use for the global searching ability. The velocity of each agent can be updated by the PSO and the acceleration of the agent is calculated by the GSA, therefore, this combination is called a hybrid PSO-GSA. The velocity and the position of the i-th agent are updated by the following two equations [96,97]:

$$v_{i,d}^{k+1} = \omega * v_{i,d}^k + C_1' * rand() * A_{i,d}^k + C_2' * rand() * \left(gbest^k - s_{i,d}^k\right) \tag{57}$$

$$s_{i,d}^{k+1} = s_{i,d}^k + v_{i,d}^{k+1} \tag{58}$$

where ω is the inertia weighting factor, $v_{i,d}^{k}$, $s_{i,d}^{k}$ and $A_{i,d}^{k}$ are the current velocity, current position, and current acceleration of the i-th particle at the k-th iteration with the d-th dimension, respectively; and C_1' and C_2' are constant acceleration coefficients, respectively.

The acceleration coefficients C_1' and C_2' can be considered as the exponential functions defined by:

$$C_i' = C_{start} * \left(\frac{C_{end}}{C_{start}} \right)^{1/(1 + iter/iter_{\max})} \quad (59)$$

where C_{start} is the initial value; C_{end} is the final value; $iter_{\max}$ is the maximum iteration number; and $iter$ is the current iteration number.

In conclusion, Figure 7 shows the basic steps in the hybrid PSO-GSA to find the optimal setting parameters of the OCRs in the DN.

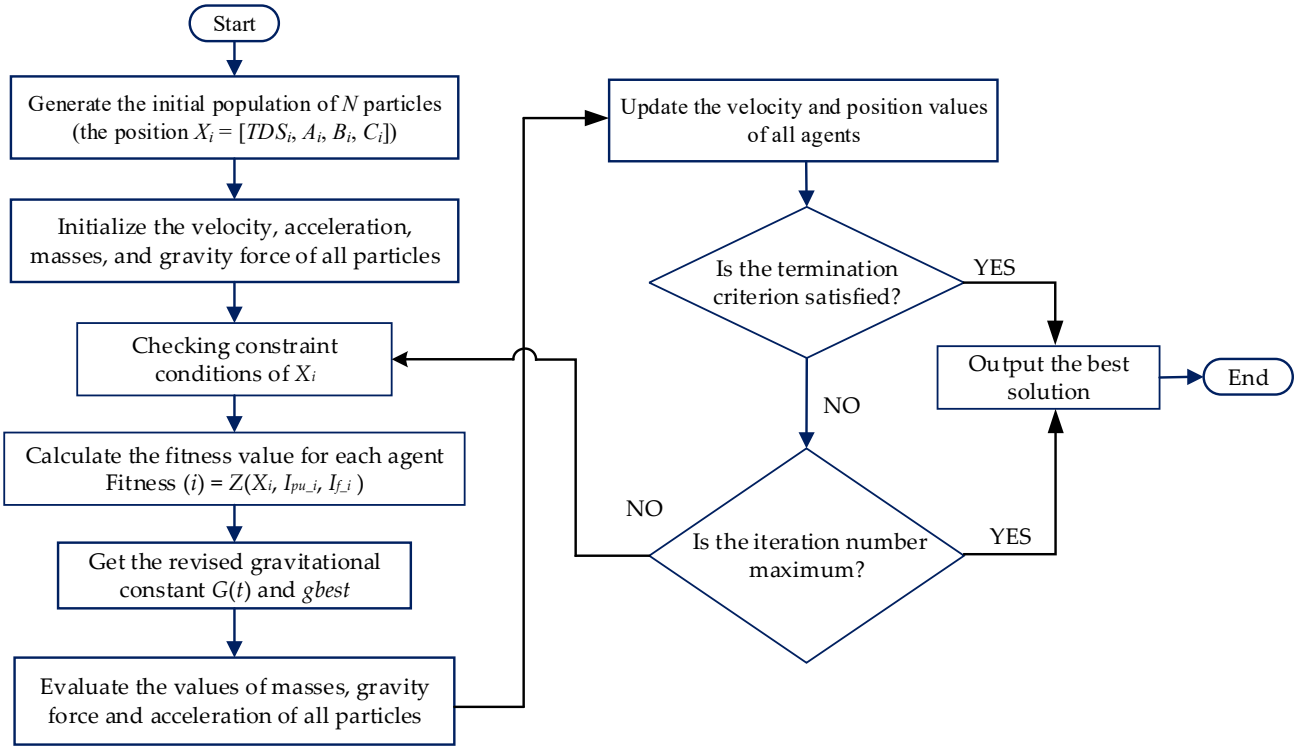

Figure 7. A flow chart of hybrid PSO-GSA applied to the proposed ASPC approach of OCRs.

2.4.3. Genetic Algorithm

The application of genetic algorithm (GA) to the ASPC approach of OCRs in the DG-based DN is shown in Figure 8. The algorithm selects the optimal TDS setting and A, B and C coefficients of protection characteristic curve. In general, the GA works in the process of biological selection, crossover, mutation and combination [98,99]. Survival of the fittest among all feasible solutions in the binary form of genes (or string structures) is considered in the GA. For each generation, a new set of potential solutions is created by the fittest of the previous set of solutions. The control variables are represented in the string structures. The GA randomly initializes the solutions, then, the fitness evaluation of each solution is performed. The fitness function is the same as the objective function Z in Equation (2) of Section 2.2. The solution has the higher fitness which can be probably selected for a new generation; this procedure is also called the biological selection or reproduction. Crossover and mutation steps are applied to get an available range of feasible solutions. When the new generation is obtained, the algorithm will repeatedly work until the termination condition is satisfied. In Figure 8, the counter of generation, G, is initially set to 1. The parameter I is defined as the counter of population, which will stop until getting the population size.

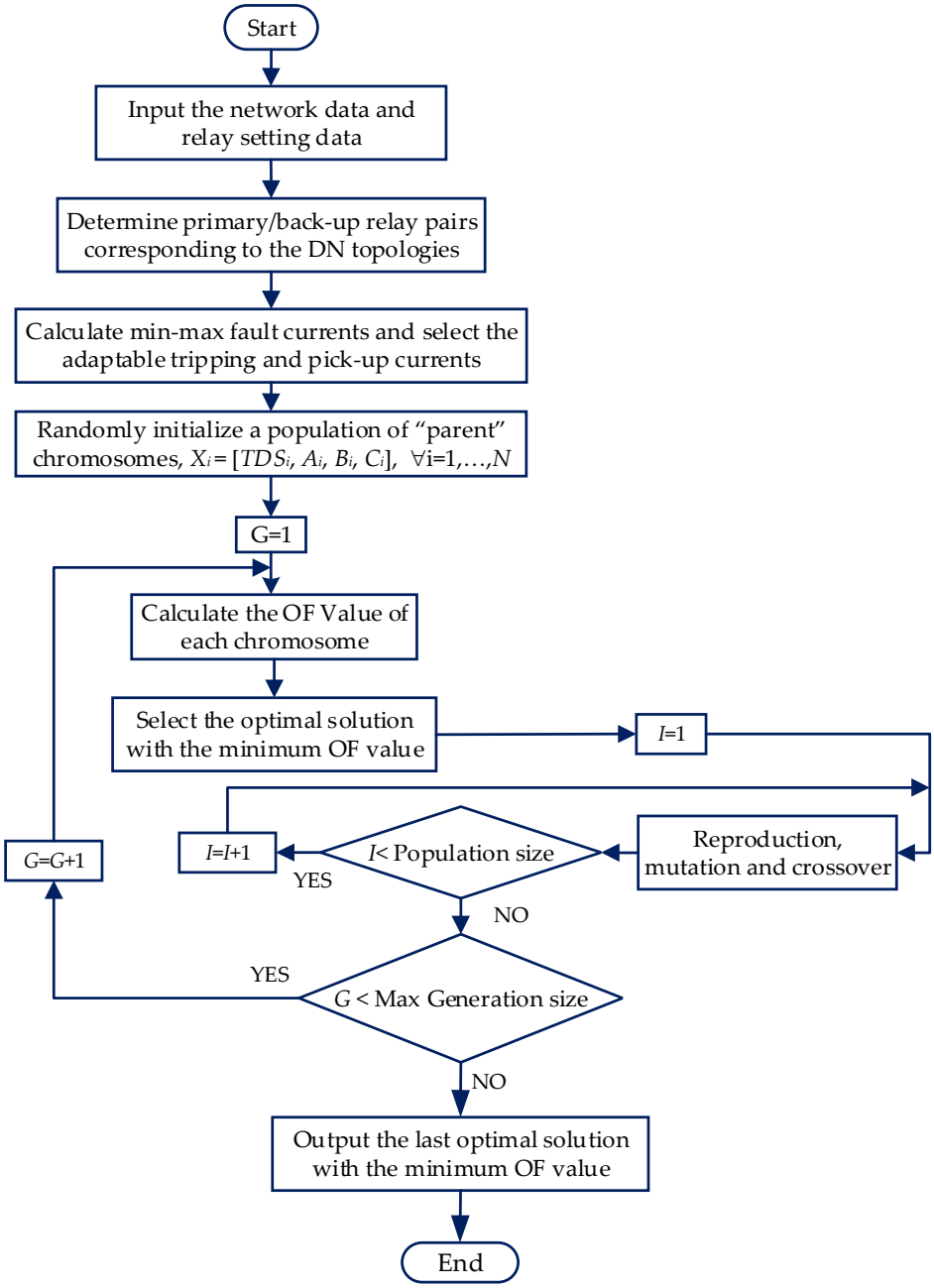

Figure 8. A flow chart of GA applied to the proposed ASPC approach of OCRs in the DN.

3. A Real 22 kV DG-Integrated Distribution Network: A Case Study

A real 22 kV DG-contained distribution network of Ho Chi Minh City, Vietnam is simulated by the ETAP software for evaluating the reliable fault analysis results and validating the proposed ASPC approach of OCRs, as seen in Figure 9. It is worth noting that the real 22 kV DG-integrated distribution network is used for this study instead of standard IEEE distribution systems. To explain that, the use of real-time load data of this DN is completely appropriate to determine the min-max confidence thresholds of load power at each load bus, the min-max confidence thresholds of load current, the min-max confidence interval of bus voltages, and the min-max confidence interval of fault currents contributed by the grid and the DG units as presented in Section 2.3.3. In the steady-state (normal) operation mode, the ASPC approach is performed to give the optimal solution of TDS multiplier and *A*, *B*, and *C* coefficients for inverse-time OC functions and to select tripping and pick-up current thresholds respectively for the definite-time and inverse-time

OC functions in the OCRs of a feeder supplied by the 110/22 kV Can-Gio power substation such as a 471 Hao-Vo OC relay, a REC Hao-Vo OC relay, and a REC Can-Thanh 163 OC relay. Moreover, the relay coordination in the real distribution network is discussed only in radial topologies. As seen in Figure 9, the feeder supplied by the 110/22 kV Can-Gio power substation is separated from the feeder supplied by the 110/22 kV An-Nghia power substation through opening a LBS (load breaker switch) Can-Thanh 97 to be operated in the radial topology. In Vietnam, the radial distribution systems are used for the normal (long-term) operation mode, while the ring-type distribution systems are only established for ancillary services or post-fault service restoration scenarios (the short-term operation mode). Therefore, the protection coordination solutions of OCRs are mostly analyzed for the radial systems, while the coordination solutions of DOC relays in the ring-type systems are limited in this case study.

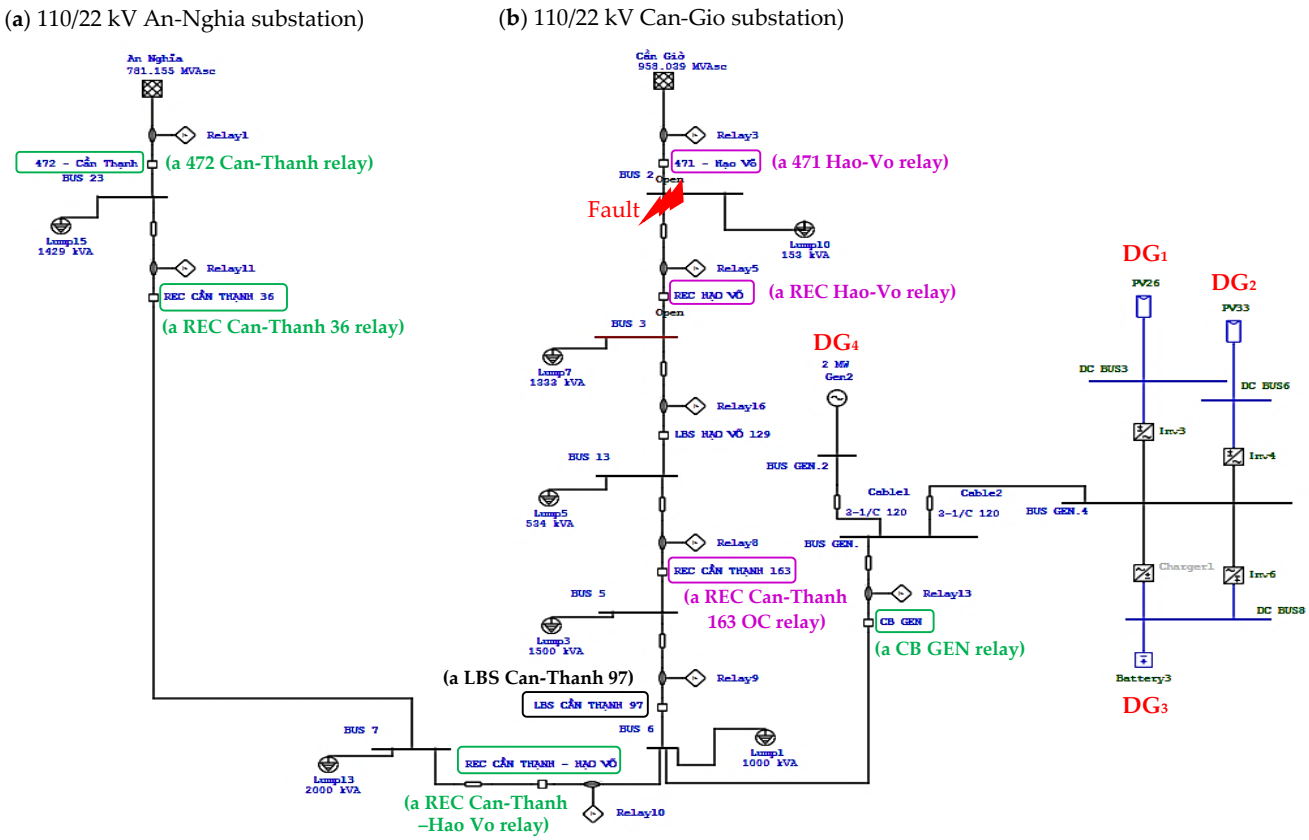

Figure 9. A real 22 kV DG-based distribution network is supplied by two power substations, namely, the 110/22 kV Can-Gio substation and the 110/22 kV An-Nghia substation, three IBDGs (DG_1, DG_2, and DG_3), and one RBDG (DG_4).

Figure 10 shows a simplified single-line diagram of the real 22 kV DG-integrated DN so that pre-fault and post-fault DN topologies can be indicated more clearly. Noted that a 3ph-G fault is given at Bus 2 of the DN. More clearly, at the pre-fault operation mode, a LBS (load breaker switch) Can-Thanh 97 is normally opened, the real 22 kV DN operates with two separate feeders. One feeder is supplied by the 110/22 kV Can-Gio power substation; and a power flow of this feeder is indicated by a dashed line (a). The other feeder is supplied by the 110/22 kV An-Nghia substation; and its power flow direction is shown by a dashed line (b). When the 3ph-G fault occurs at Bus 2, a 471 Hao-Vo relay and a REC Hao-Vo relay will give the tripping signals to the related circuit breakers, namely a 471 Hao-Vo circuit breaker and a REC Hao-Vo recloser, to isolate the fault at Bus 2. After clearing the fault, according to the proposed FISR plans [10,11], the protection coordination results of the related OCRs will be updated by the ASPC system through the SCADA function. By specifically considering the given fault at Bus 2, there are three feasible FISR plans which will be the basis to find the optimal parameter settings of the related OCRs. The first FISR

plan is to use an adjacent distribution feeder to restore the power for interrupted customers through closing the LBS Can-Thanh 97 device and opening a circuit breaker controlled by a CB GEN relay. The power flow direction of the first FISR plan is indicated by a dashed line (c). The second FISR plan is to use three IBDGs and one RBDG in the DN as ancillary services. DG_1 and DG_2 are the 0.5 MWp photovoltaic (PV) generation systems. DG_3 is a 7.3 MWh and 1 MW battery energy storage system (BESS). DG_4 is a 2 MW diesel generator. The second FISR plan is performed by closing the LBS Can-Thanh 97 device and the CB of DG sources while opening the REC Can-Thanh Hao-Vo recloser. The power flow direction of the second FISR plan is represented by a dashed line (d). The last FISR plan is to use both the neighboring distribution feeder and all DG sources. The power flow direction of the last plan is followed by the two dashed lines (c) and (d). As a result, the ASPC approach should give at least three optimal protection coordination solutions for the related OCRs corresponding to the three above FISR plans in the case of the 3ph-G fault that occurred at Bus 2 of the real 22 kV DN.

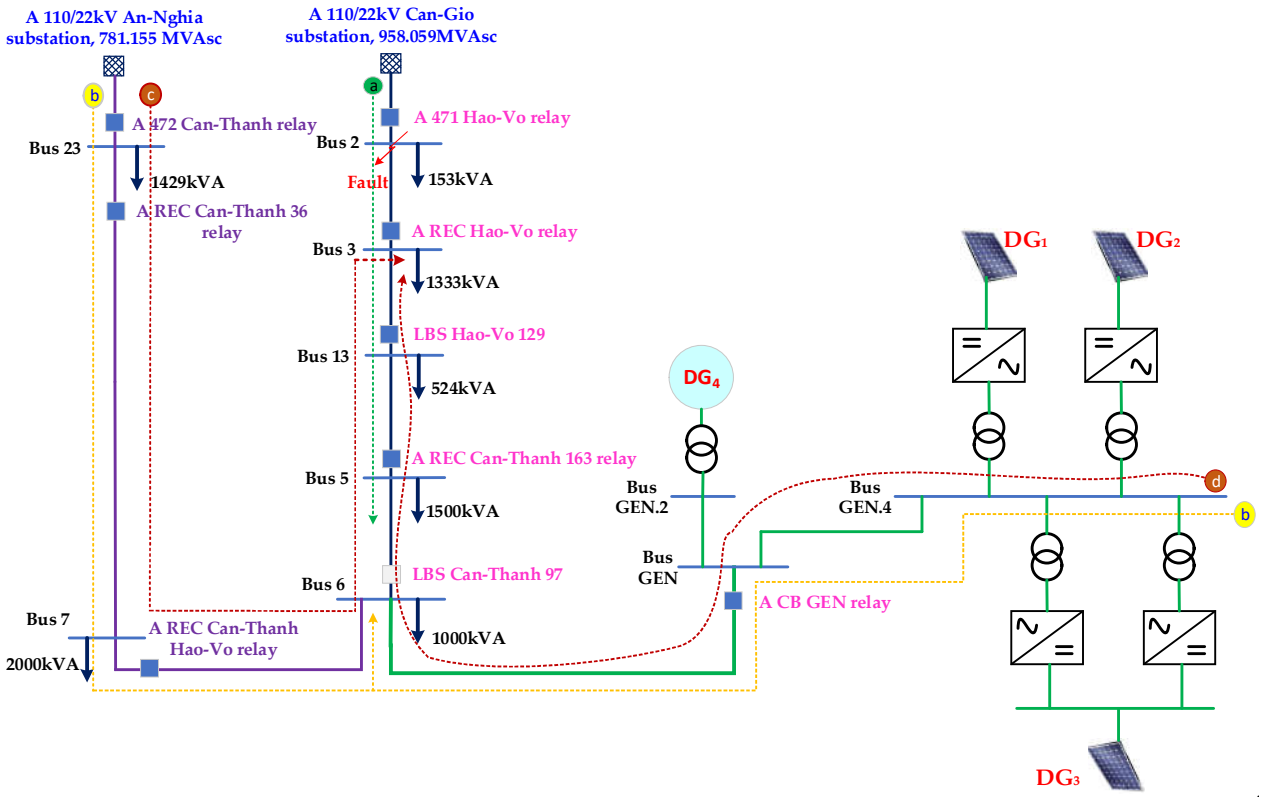

Figure 10. A simplified single-line diagram of the real 22 kV DG-integrated DN.

4. Overcurrent Protection Coordination Results, Analysis and Discussion

4.1. Reliable Fault-Current Calculation Results

As summarized from Section of An Adaptable Fault Analysis Technique, instead of using a fixed fault-current value for each fault type with the unconsidered reliability, this paper has contributed an adaptable fault analysis technique to calculate the min-max confidence interval of fault current for each different fault type. The maximum and minimum confidence thresholds of fault current are used to select tripping and pick-up thresholds of definite-time and inverse-time OC functions in the OCR of the DG-integrated DN, respectively. By considering a feeder only supplied by the 110/22 kV Can-Gio power substation from a real 22 kV DG-based distribution network, Table 2 shows the fault analysis results of this feeder. It is noted that Bus 5 is the end bus of the feeder. Three OC relays are used to protect this feeder including a 471 Hao-Vo OCR, a REC Hao-Vo OCR, and a REC Can-Thanh 163 OCR. The maximum fault currents can be seen by the OCRs in the

DN when the various fault types occur at their protected zones/lines. Specifically, the REC Can-Thanh 163 OCR operates as the primary protection for faults at Bus 5. The maximum fault-current value of each fault type such as 3ph-G, 2ph-G, ph-ph and 1ph-G faults at Bus 5 is seen by this REC Can-Thanh 163 OCR, which is also shown in Table 2. Similarly, the REC Hao-Vo OCR operates as the primary protection for faults at Bus 13. The maximum fault-current value of each fault type such as 3ph-G, 2ph-G, ph-ph and 1ph-G faults at Bus 13 is seen by this REC Hao-Vo OCR. In addition, the 471 Hao-Vo OCR operates as the primary protection for faults at Bus 2. The maximum fault-current value of each fault type such as 3ph-G, 2ph-G, ph-ph and 1ph-G faults at Bus 2 is seen by this 471 Hao-Vo OCR.

Table 2. Numerical fault-current calculation results are seen by the OCRs in a considered feeder of the DG-based DN.

Fault Types	Maximum Fault Currents Detected by the OCRs		
	Maximum Fault Currents at Bus 2 Are Detected by a 471 Hao-Vo OCR	**Maximum Fault Currents at Bus 13 Are Detected by a REC Hao-Vo OCR**	**Maximum Fault Currents at Bus 5 Are Detected by a REC Can-Thanh 163 OCR**
3ph-G fault	25,796 A	11,911 A	4902 A
2ph-G fault	24,347 A	10,742 A	4426 A
1ph-G fault	22,340 A	10,316 A	4246 A
ph-ph fault	20,469 A	6488 A	2340 A

As mentioned in Section 3, after a 3ph-G fault at Bus 2 of the feeder is cleared, three feasible FISR plans are proposed. Table 3 presents the maximum fault-current calculation results observed by the OCRs corresponding to four different operating scenarios of the DN, including:

- Scenario 1–the DN topology before the fault occurs at Bus 2, i.e., the feeder supplied by the 110/22 kV Can-Gio power substation, as referred to the dashed line (a) in Figure 10.
- Scenario 2–the DN topology for the first FISR plan, as referred to the dashed line (c) in Figure 10.
- Scenario 3–the DN topology for the second FISR plan, as referred to the dashed line (d) in Figure 10.
- Scenario 4–the DN topology for the third FISR plan, as referred to the two dashed lines (c) and (d) in Figure 10.

Moreover, the OCR triple for each topology including one primary relay and two backup relays is also shown in Table 3. It is noted that some faulted locations can be only detected and cleared by the OCR pairs. The maximum fault-current values which are calculated from four different fault types at the buses of the real 22 kV distribution network are indicated in this table by an order-based format, specifically [$the\ maximum\ 3ph-G\ fault\ current$;$the\ maximum\ 2ph-G\ fault\ current$;$the\ maximum\ 1ph-G\ fault\ current$; $the\ maximum\ ph-ph\ fault\ current$].

Table 3. Numerical fault-current calculation results are detected by the OCRs corresponding to four different operation scenarios of the real 22 kV distribution network.

(a) Scenario 1–A DN topology before the fault occurs at Bus 2: The LBS Can-Thanh 97 is normally opened; and the feeder is only supplied by the 110/22 kV Can-Gio power substation.		
Faults at Bus 2	**Faults at Bus 13**	**Faults at Bus 5**
Primary protection: the 471 Hao-Vo OCR	*Primary protection*: the REC Hao Vo OCR	*Primary protection*: the REC Can-Thanh 163 OCR
Backup protection: None	*Backup protection*: the 471 Hao-Vo OCR	*Backup protection*: the REC Hao-Vo OCR and the 471 Hao-Vo OCR
Maximum fault currents at Bus 2 are detected by the 471 Hao-Vo OCR: [25.8; 24.3; 22.3; 20.4] kA	Maximum fault currents at Bus 13 are detected by the REC Hao-Vo OCR: [11.9; 10.7; 10.3; 6.5] kA	Maximum fault currents at Bus 5 are detected by the REC Can-Thanh 163 OCR: [4.9; 4.4; 4.2; 2.3] kA
(b) Scenario 2–A DN topology for the first FISR plan: As referred to the dashed line (c) in Figure 10; the REC Hao-Vo recloser is opened to isolate the fault at Bus 2; then the LBS Can-Thanh 97 is closed; and a CB GEN of DG sources is still opened.		
Faults at Bus 7	**Faults at Bus 5**	**Faults at Bus 3**
Primary protection: the REC Can-Thanh 36 OCR	*Primary protection*: the REC Can Thanh–Hao Vo OCR	*Primary protection*: the REC Can-Thanh 163 OCR
Backup protection: the 472 Can-Thanh OCR	*Backup protection*: the REC Can Thanh 36 OCR and the 472 Can-Thanh OCR	*Backup protection*: the REC Can Thanh–Hao Vo OCR and the REC Can Thanh 36 OCR
Maximum fault currents at Bus 7 are detected by the REC Can-Thanh 36 OCR: [21.5; 21.4; 20.1; 18.6] kA	Maximum fault currents at Bus 5 are detected by the REC Can Thanh–Hao Vo OCR: [3.2; 2.8; 2.7; 1.3] kA	Maximum fault currents at Bus 3 are detected by the REC Can-Thanh 163 OCR: [2.6; 2.4; 2.2; 1.15] kA
(c) Scenario 3–A DN topology for the second FISR plan: As referred to the dashed line (d) in Figure 10; the REC Hao-Vo recloser is opened to isolate the fault at Bus 2; the REC Can Thanh–Hao Vo recloser is opened; and then a CB GEN of DG sources is closed.		
Faults at Bus 5		**Faults at Bus 3**
Primary protection: the OCR at the CB GEN		*Primary protection*: the REC Can-Thanh 163 OCR
Backup protection: None		*Backup protection*: the OCR at the CB GEN
Maximum fault currents at Bus 5 are detected by the OCR at the CB GEN: [1.1; 1.0; 0.9; 0.8] kA		Maximum fault currents at Bus 3 are detected by the REC Can-Thanh 163 OCR: [0.85; 0.80; 0.75; 0.70] kA
(d) Scenario 4–A DN topology for the third FISR plan: As referred to the two dashed lines (c) and (d) in Figure 10; the REC Hao-Vo recloser is opened to isolate the fault at Bus 2; and then both the REC Can Thanh–Hao Vo recloser and the CB GEN are simultaneously closed.		
Faults at Bus 7	**Faults at Bus 5**	**Faults at Bus 3**
Primary protection: the REC Can-Thanh 36 OCR	*Primary protection*: the REC Can Thanh–Hao Vo OCR and the CB GEN OCR	*Primary protection*: the REC Can-Thanh 163 OCR
Backup protection: the 472 Can-Thanh OCR	*Backup protection*: the REC Can-Thanh 36 OCR and the 472 Can-Thanh OCR	*Backup protection*: the OCR at CB GEN, the REC Can Thanh–Hao Vo OCR, and the REC Can-Thanh 36 OCR
Maximum fault currents at Bus 7 are detected by the REC Can-Thanh 36 OCR: [21.7; 21.6; 20.4; 18.8] kA	Maximum fault currents at Bus 5 are detected by the REC Can Thanh–Hao Vo OCR: [3.4; 3.1; 3.0; 1.8] kA and by the OCR at the CB GEN: [0.85; 0.80; 0.75; 0.70] kA	Maximum fault currents at Bus 3 are detected by the REC Can-Thanh 163 OCR: [2.9; 2.7; 2.6; 1.7] kA

4.2. Protection Coordination Results in Scenario 1

Optimal protection coordination results of the OCRs in Scenario 1 which are calculated by the GA, GSA and hybrid PSO-GSA are indicated in Table 4. In this table, I_f is the

tripping-current threshold selected for the 50P and 50G functions of the OCRs, as referred to Section 2.3.5. $t_{trip}^{defined}$ is the pre-defined tripping time of the 50P and 50G functions of the OCRs. Moreover, the TDS multiplier and A, B, and C coefficients of the 51P and 51G OC functions of the OCRs are shown in the table. It is noted that the CTI is selected to 0.30~0.35 s. For example, when a 3ph-G fault is at Bus 2, the 471 Hao-Vo relay is the primary relay while there is not any backup relay. The tripping time of the 471 Hao-Vo relay is 0.01 s to clear the fault at Bus 2. On the other hand, when a typical 3ph-G fault is given at the end point of the feeder (at Bus 5) as referred to a dashed line (a) in Figure 10, the REC Can-Thanh 163 OCR is the primary relay while the REC Hao-Vo relay and the 471 Hao-Vo relay are the backup relays. Based on the optimal setting parameters obtained by the ASPC system for these OCRs, their tripping time t_{trip} to clear the fault at Bus 5 are also indicated in Table 4. The results have demonstrated that the CTI constraints from Equations (3)–(5) are completely satisfied.

Table 4. Optimal protection coordination results of the OCRs in Scenario 1 and their tripping time when the fault is at Bus 5.

The OCRs	50P		50G		51P				51G			
						GA	GSA	PSO-GSA		GA	GSA	PSO-GSA
The 471 Hao-Vo OCR	I_f	20,469 A	I_f	22,340 A	A	13.06	57.94	68.34	A	50.75	89.14	93.49
					B	2.14	2.44	2.49	B	2.12	2.31	2.50
					C	1.11	0.38	1.43	C	0.71	0.83	1.48
	$t_{trip}^{defined}$	0.01 s	$t_{trip}^{defined}$	0.01 s	TDS	0.41	0.33	0.21	TDS	0.067	0.05	0.05
					The tripping time of the relay for the typical fault at Bus 5:							
					t_{trip}	0.62 s	0.61 s	0.62 s	t_{trip}	0.62 s	0.61 s	0.62 s
The REC Hao-Vo OCR	I_f	6488 A	I_f	10316 A	A	36.23	72.58	5.81	A	78.07	74.84	13.74
					B	1.32	2.42	2.50	B	2.36	2.32	2.37
					C	1.07	0.22	0.00	C	0.25	0.53	0.00
	$t_{trip}^{defined}$	0.01 s	$t_{trip}^{defined}$	0.01 s	TDS	0.05	0.15	2.24	TDS	0.03	0.03	0.17
					The tripping time of the relay for the typical fault at Bus 5:							
					t_{trip}	0.32 s	0.31 s	0.31 s	t_{trip}	0.32 s	0.31 s	0.31 s
The REC Can-Thanh 163 OCR	I_f	2340 A	I_f	4246 A	A	0.036	59.36	0.01	A	3.95	59.97	0.01
					B	2.14	2.31	0.48	B	2.39	2.29	1.72
					C	1.00	0.01	0.00	C	0.3	0.72	0.01
	$t_{trip}^{defined}$	0.01 s	$t_{trip}^{defined}$	0.01 s	TDS	0.01	0.01	1.17	TDS	0.01	0.01	0.01
					The tripping time of the relay for the typical fault at Bus 5:							
					t_{trip}	0.01 s	0.01 s	0.01 s	t_{trip}	0.01 s	0.01 s	0.01 s

Figure 11 shows the optimal protection characteristic curves of the OC relays in Scenario 1 of the DN. Regarding the obtained coordination results of 51P/G and 50P/G functions, Relay 1 represents the OC protection function embedded into the REC Can-Thanh 163 recloser; Relay 2 represents the OC protection function integrated into the REC Hao-Vo recloser; and Relay 3 indicates the OC protection function used to control the 471 Hao-Vo circuit breaker. When the 3ph-G fault occurs at Bus 2, the maximum 3ph-G fault current is 25.8 kA as shown in Table 3, so the 471 Hao-Vo OCR only takes 0.01 s to send a tripping signal to the 471 Hao-Vo CB. When the 3ph-G fault occurs at Bus 5, the maximum 3ph-G fault current is 4.9 kA as indicated in Table 3, so the primary operation time of the REC Can-Thanh 163 OCR is 0.01 s, the backup operation times of the REC Hao-Vo OCR and the 471 Hao-Vo OCR are 0.31 s~0.32 s and 0.61 s~0.62 s, respectively, according to results of three different algorithms as seen at the table and the left-side of Figure 11. Additionally, I_{trip} represents the tripping-current threshold of 50P/G functions of the REC Can-Thanh 163 OCR. It can be observed that the characteristic curves of 51P/G functions in the OCR are certainly followed by the exponential function. However, there is a proposed protection combination of 51P/G and 50P/G functions, the inverse-time characteristic curves of 51P/G functions are terminated at the tripping-current threshold of

50P/G functions. In other words, in the same OCR, the 51P/G functions will be neglected when the fault current exceeds the tripping-current threshold of 50P/G functions. That could be an interesting contribution of this study regarding the coordination combination of 51P/G and 50P/G functions. For example, when considering the REC Hao-Vo OCR, the tripping current I_f of its 50P function is set to 6488 A as shown in Table 4. Therefore, this tripping current is considered as a terminated point of the inverse-time characteristic curve of the 51P function in the same REC Hao-Vo OCR. That can be clearly illustrated by the curve of Relay 2, i.e., a red curve of the plots at the right-side of Figure 11.

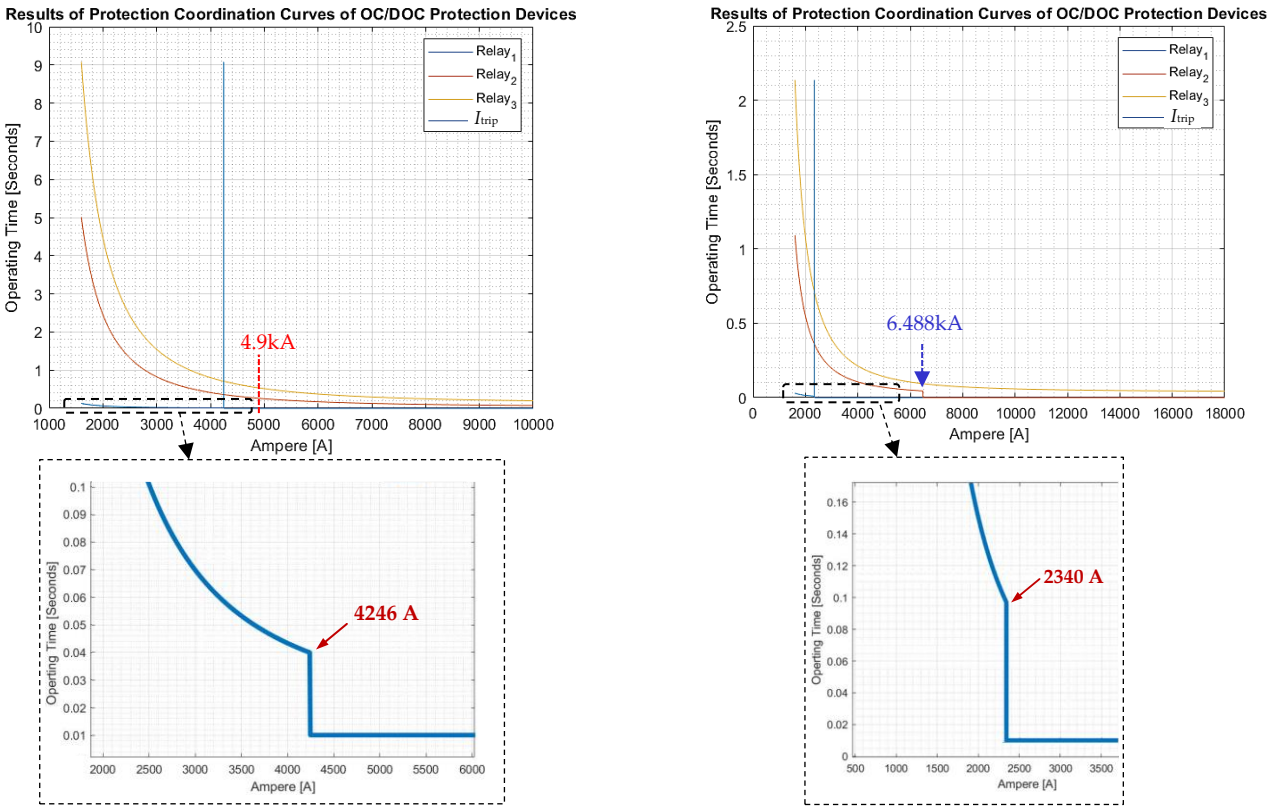

(**a**) The OC protection coordination results of 50G and 51G functions (at the left-side) and 50P and 51P functions (at the right-side) are obtained by the GSA.

Figure 11. *Cont.*

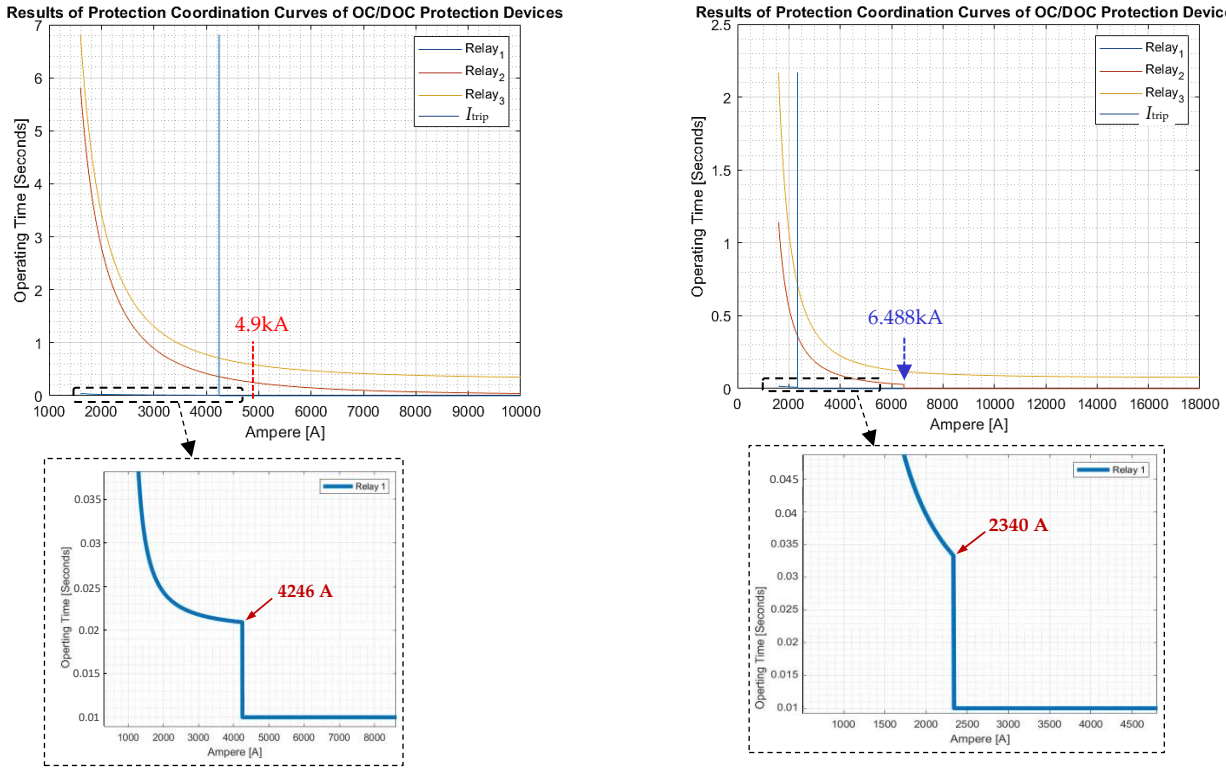

(**b**) The OC protection coordination results of 50G and 51G functions (at the left-side) and 50P and 51P functions (at the right-side) are obtained by the hybrid PSO-GSA.

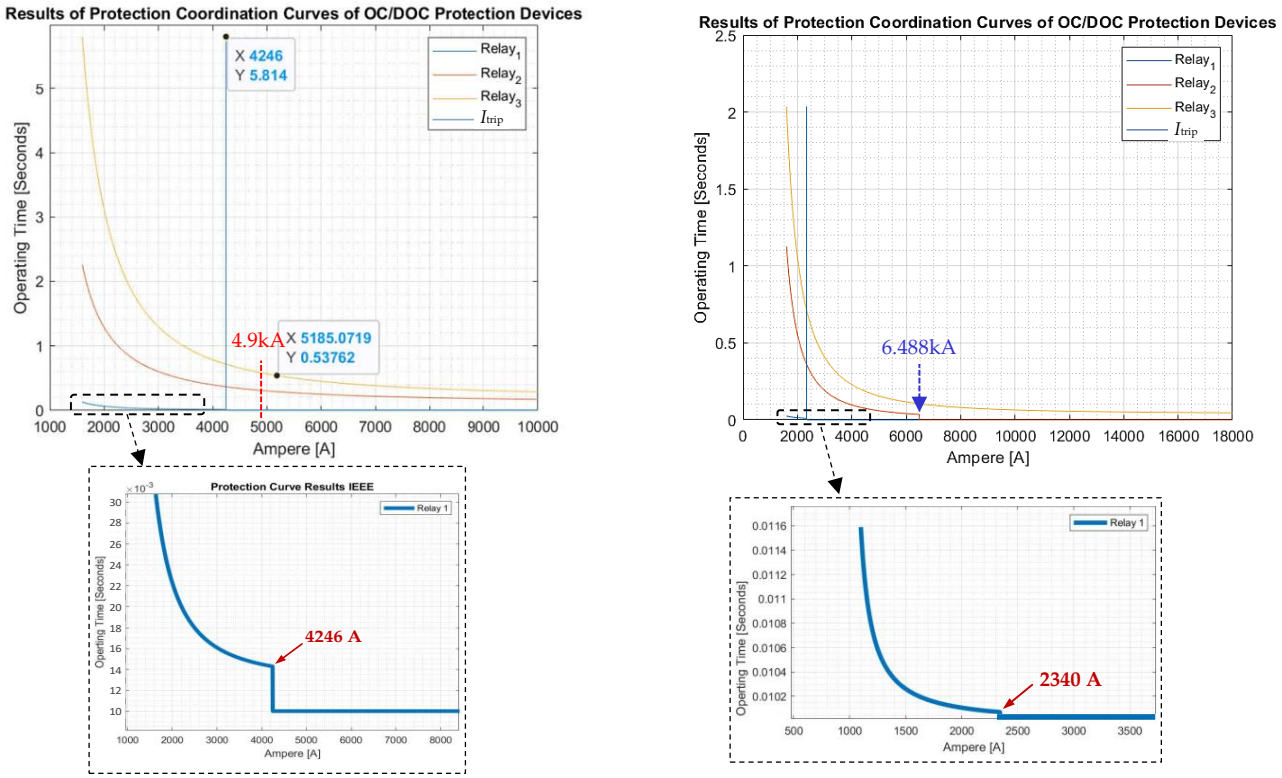

(**c**) The OC protection coordination results of 50G and 51G functions (at the left-side) and 50P and 51P functions (at the right-side) are obtained by the GA.

Figure 11. Optimal protection characteristic curves of the OC relays in Scenario 1 of the 22 kV distribution system.

4.3. Protection Coordination Results in Scenario 2

Scenario 2 is a distribution network topology of the first FISR plan after the 3ph-G fault at Bus 2 is cleared. As referred to the dashed line (c) in Figure 10, the REC Hao-Vo recloser is opened to isolate the fault at Bus 2. Then the LBS Can-Thanh 97 is closed to restore the power of interrupted customers while a CB GEN circuit breaker of DG sources is still opened. The optimal protection coordination results of the OCRs in Scenario 2 which are calculated by the GA, GSA and hybrid PSO-GSA are indicated in Table 5. In this table, I_f is the tripping-current threshold selected for the 50P and 50G functions of the OCRs including the REC Can-Thanh 36 OCR, the REC Can-Thanh Hao-Vo OCR, and the REC Can-Thanh 163 OCR. $t_{trip}^{defined}$ is the pre-defined tripping time of the 50P and 50G functions of these OCRs. Moreover, the TDS multiplier and A, B, and C coefficients of the 51P and 51G OC functions of the OCRs are shown in the table. The CTI is still selected to 0.30~0.35 s. It is worth noting that the parameter settings of the REC Can-Thanh 163 OCR must be simultaneously updated to be adaptable to Scenario 2 instead of Scenario 1. To validate the optimal setting parameters obtained by the ASPC system for the above OCRs, a 3ph-G fault is given at Bus 3. The REC Can-Thanh 163 OCR is the primary relay to detect and clear this fault while the REC Can-Thanh 36 OCR and the REC Can-Thanh Hao-Vo OCR operate as the backup relays. Their tripping time t_{trip} to clear the fault at Bus 3 are also indicated in Table 5. The achieved results have demonstrated that the CTI constraints from Equations (3)–(5) are completely satisfied.

Table 5. Optimal protection coordination results of the OCRs in Scenario 2 and their tripping time when the fault is at Bus 3.

The OCRs	50P		50G		51P				51G			
						GA	GSA	PSO-GSA		GA	GSA	PSO-GSA
The REC Can-Thanh 36 OCR	I_f	18,595 A	I_f	20,076 A	A	6.71	52.45	126.51	A	9.23	33.59	73.50
					B	2.31	2.31	2.07	B	1.74	1.82	2.50
					C	0.09	0.93	0.02	C	0.11	0.98	1.50
	$t_{trip}^{defined}$	0.01 s	$t_{trip}^{defined}$	0.01 s	TDS	0.73	0.09	0.03	TDS	0.024	0.01	0.01
					The tripping time of the relay for the typical fault at Bus 3:							
					t_{trip}	0.65 s	0.62 s	0.65 s	t_{trip}	0.65 s	0.62 s	0.65 s
The REC Can-Thanh Hao-Vo OCR	I_f	1286 A	I_f	2755 A	A	7.77	44.37	0.60	A	0.01	30.55	0.01
					B	2.46	1.79	2.28	B	0.60	2.19	1.75
					C	0.47	0.28	0.02	C	0.89	0.79	0.74
	$t_{trip}^{defined}$	0.01 s	$t_{trip}^{defined}$	0.01 s	TDS	0.26	0.03	1.26	TDS	0.37	0.01	0.46
					The tripping time of the relay for the typical fault at Bus 3:							
					t_{trip}	0.33 s	0.32 s	0.33 s	t_{trip}	0.33 s	0.32 s	0.33 s
The REC Can-Thanh 163 OCR	I_f	1167 A	I_f	2501 A	A	0.09	60.60	0.01	A	0.01	0.74	0.01
					B	0.44	2.33	1.39	B	1.51	0.89	2.06
					C	0.30	0.46	0.00	C	0.97	0.87	0.01
	$t_{trip}^{defined}$	0.01 s	$t_{trip}^{defined}$	0.01 s	TDS	0.03	0.01	3.00	TDS	0.01	0.01	0.43
					The tripping time of the relay for the typical fault at Bus 3:							
					t_{trip}	0.01 s	0.01 s	0.01 s	t_{trip}	0.01 s	0.01 s	0.01 s

Figure 12 shows the optimal protection characteristic curves of the OC relays in Scenario 2 of the DN. Regarding the obtained coordination results of 51P/G and 50P/G functions, Relay 1 represents the OC protection function embedded into the REC Can-Thanh 163 recloser; Relay 2 represents the OC protection function integrated into the REC Can-Thanh Hao-Vo recloser; and Relay 3 indicates the OC protection function used to control the REC Can-Thanh 36 recloser. When the 3ph-G fault occurs at Bus 3, the maximum 3ph-G fault current is 2.6 kA as indicated in Table 3, so the primary operation time of the REC Can-Thanh 163 OCR is 0.01 s. The backup operation times of the REC Can-Thanh Hao-Vo OCR and the REC Can-Thanh 36 OCR are 0.32~0.33 s and 0.62~0.65 s, respectively, according to results of three different algorithms as seen at the table and the left-side of Figure 12. Additionally, I_{trip} represents the

tripping-current threshold of 50P/G protection functions of the REC Can-Thanh 163 OCR. By further considering the REC Can-Thanh 163 OCR, the tripping current I_f of its 50G function is set to 2501 A as shown in Table 5. Thus, this tripping current is considered as a terminated point of the inverse-time characteristic curve of the 51G function in the same REC Can-Thanh 163 OCR. Similarly, the tripping current I_f of the 50G function of the REC Can-Thanh Hao-Vo OCR which is 2755 A is considered as a finishing point of the inverse-time characteristic curve of its 51G function, as clearly illustrated by the curve of Relay 2, i.e., a red curve of the plots at the left-side of Figure 12.

4.4. Protection Coordination Results in Scenario 3

Scenario 3 is a distribution network topology of the second FISR plan after the 3ph-G fault at Bus 2 is cleared. As referred to the dashed line (d) in Figure 10, the REC Hao-Vo recloser is opened to isolate the fault at Bus 2. Then the LBS Can-Thanh 97 is closed to restore the power of interrupted customers while the REC Can-Thanh–Hao-Vo recloser is opened and a CB GEN circuit breaker of DG sources is closed. The optimal protection coordination results of the OCRs in Scenario 3 which are calculated by the GA, GSA and hybrid PSO-GSA are indicated in Table 6. In this table, I_f is the tripping-current threshold selected for the 50P and 50G functions of the OCRs including the CB GEN OCR and the REC Can-Thanh 163 OCR. $t_{trip}^{defined}$ is the pre-defined tripping time of the 50P and 50G functions of these OCRs. Moreover, the TDS multiplier and A, B, and C coefficients of the 51P and 51G OC functions of the above OCRs are shown in the table. The CTI is still selected to 0.30~0.35 s. It is worth noting that the parameter settings of the REC Can-Thanh 163 OCR must be simultaneously updated to be adaptable to Scenario 3 instead of Scenario 1 or Scenario 2. To validate the optimal setting parameters obtained by the ASPC system for the above OCRs, a 3ph-G fault is given at Bus 3. The REC Can-Thanh 163 OCR operates as the primary protection to detect and clear this fault while the CB GEN OCR operates as the backup protection. Their tripping time t_{trip} to clear the fault at Bus 3 are also indicated in Table 6. The achieved results have demonstrated that the CTI constraints from Equations (3)–(5) are completely satisfied.

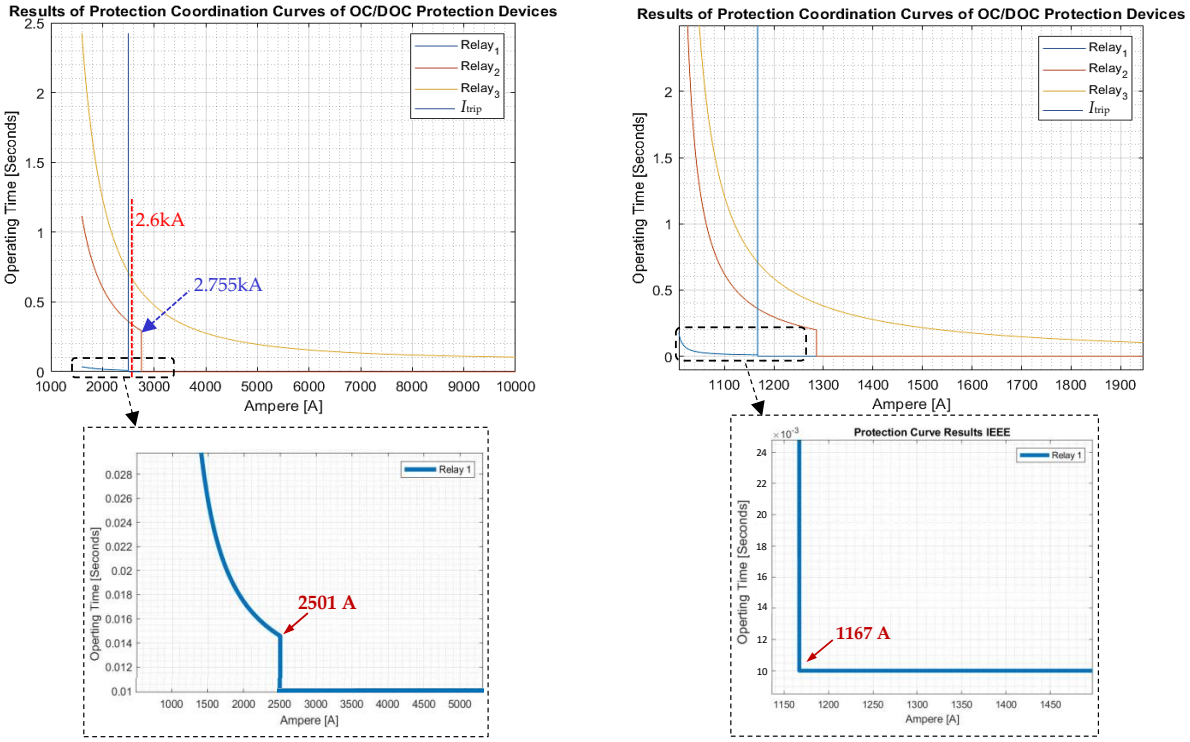

(**a**) The OC protection coordination results of 50G and 51G functions (at the left-side) and 50P and 51P functions (at the right-side) are obtained by the GSA.

Figure 12. *Cont.*

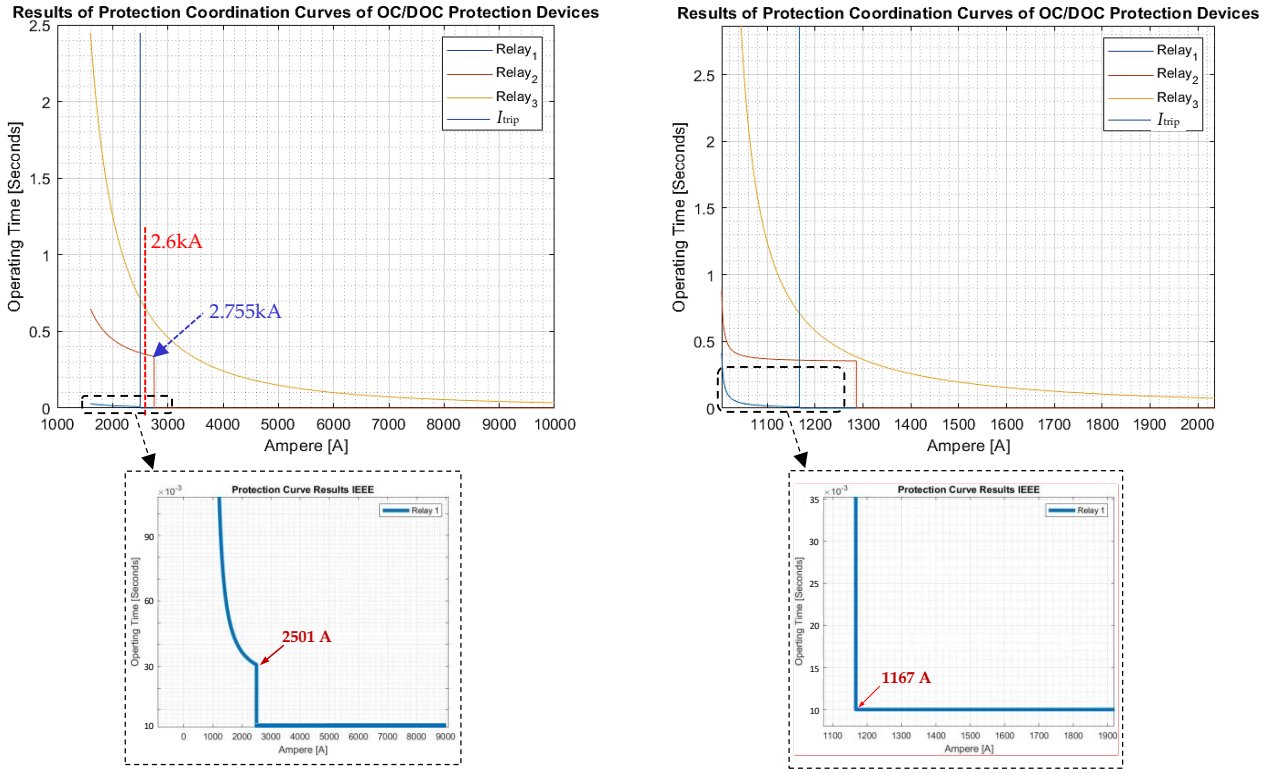

(**b**) The OC protection coordination results of 50G and 51G functions (at the left-side) and 50P and 51P functions (at the right-side) are obtained by the hybrid PSO-GSA.

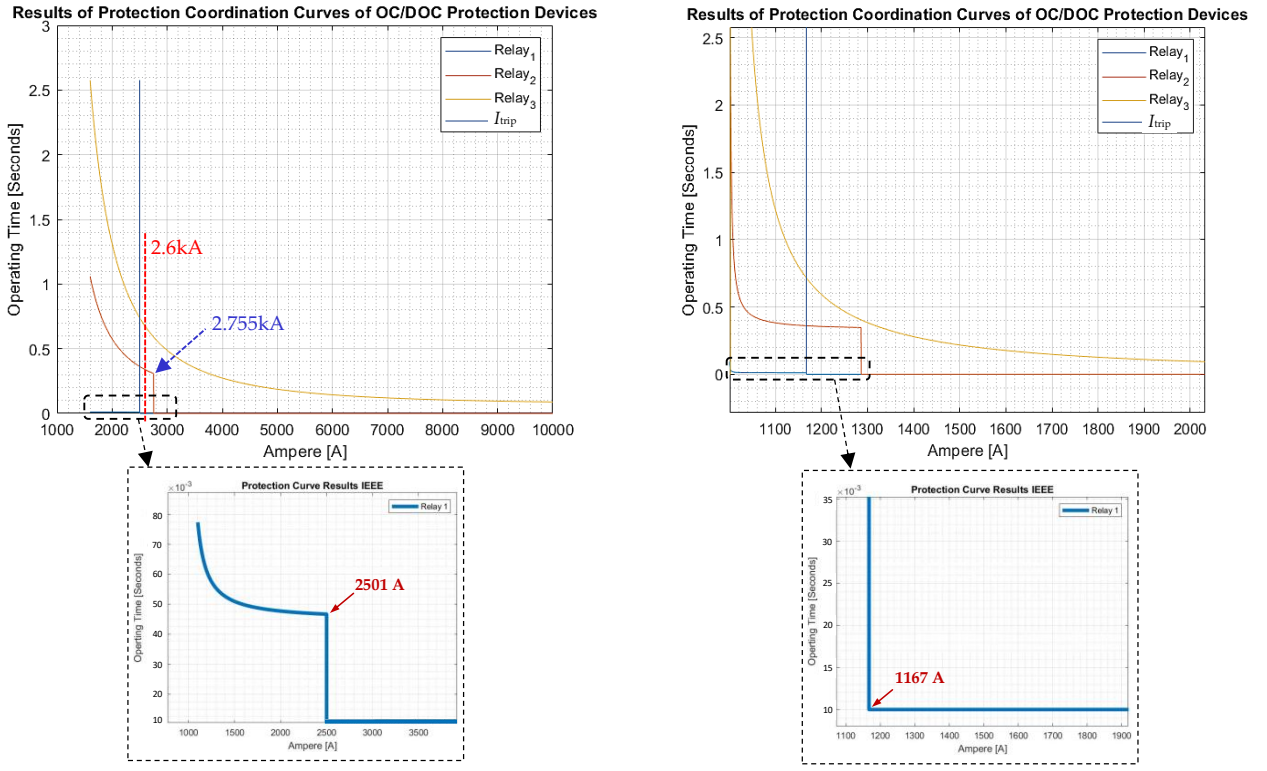

(**c**) The OC protection coordination results of 50G and 51G functions (at the left-side) and 50P and 51P functions (at the right-side) are obtained by the GA.

Figure 12. Optimal protection characteristic curves of the OC relays in Scenario 2 of the 22 kV distribution system.

Table 6. Optimal protection coordination results of the OCRs in Scenario 3 and their tripping time when the fault is at Bus 3.

The OCRs	50P		50G		51P				51G			
						GA	GSA	PSO-GSA		GA	GSA	PSO-GSA
A CB GEN OCR	I_f	816 A	I_f	910 A	A	4.39	57.46	0.01	A	0.23	67.95	0.01
					B	2.41	2.17	2.50	B	2.45	2.24	2.25
					C	1.18	0.59	0.05	C	0.76	0.80	0.80
	$t_{trip}^{defined}$	0.01 s	$t_{trip}^{defined}$	0.01 s	TDS	0.09	0.01	7.16	TDS	0.35	0.01	0.45
					The tripping time of the relay for the typical fault at Bus 3:							
					t_{trip}	0.35 s	0.32 s	0.35 s	t_{trip}	0.35 s	0.32 s	0.35 s
The REC Can-Thanh 163 OCR	I_f	700 A	I_f	750 A	A	1.11	59.93	0.01	A	0.01	47.43	0.01
					B	2.03	2.05	2.31	B	2.45	2.22	2.50
					C	0.00	0.81	0.01	C	1.01	0.66	0.00
	$t_{trip}^{defined}$	0.01 s	$t_{trip}^{defined}$	0.01 s	TDS	0.01	0.01	0.69	TDS	0.01	0.01	1.02
					The tripping time of the relay for the typical fault at Bus 3:							
					t_{trip}	0.01 s	0.01 s	0.01 s	t_{trip}	0.01 s	0.01 s	0.01 s

4.5. Protection Coordination Results in Scenario 4

Scenario 4 is a distribution network topology of the third FISR plan after the 3ph-G fault at Bus 2 is cleared. As referred to the two dashed lines (c) and (d) in Figure 10, the REC Hao-Vo recloser is opened to isolate the fault at Bus 2. The LBS Can-Thanh 97 is then closed to restore the power of interrupted customers while the REC Can-Thanh–Hao-Vo recloser and the CB GEN circuit breaker are closed to allow the interlinking operation of both the feeder supplied by the 110/22 kV An-Nghia power substation and the other feeder supplied by the DG sources. The optimal protection coordination results of the OCRs in Scenario 4 which are calculated by the GA, GSA and hybrid PSO-GSA are indicated in Table 7. In this table, I_f is the tripping-current threshold selected for the 50P and 50G functions of the OCRs including the REC Can-Thanh 36 OCR, the REC Can-Thanh–Hao-Vo OCR, the CB GEN OCR and the REC Can-Thanh 163 OCR. $t_{trip}^{defined}$ is the pre-defined tripping time of the 50P and 50G functions of these OCRs. Moreover, the TDS multiplier and A, B, and C coefficients of the 51P and 51G OC functions of the above OCRs are shown in the table. The CTI is still selected to 0.30~0.35 s. It is worth noting that the parameter settings of the REC Can-Thanh 163 OCR must be simultaneously updated to be adaptable to Scenario 4 instead of Scenario 1, Scenario 2, or Scenario 3. To validate the optimal setting parameters obtained by the ASPC system for the above OCRs, a 3ph-G fault is given at Bus 3. The REC Can-Thanh 163 OCR operates as the primary protection to detect and clear this fault while the CB GEN OCR operates as the backup protection on the feeder supplied by the DG sources and the REC Can-Thanh 36 OCR and the REC Can-Thanh–Hao-Vo OCR are the backup relays on the other feeder supplied by the 110/22 kV An-Nghia power substation. Their tripping time t_{trip} to clear the 3ph-G fault at Bus 3 are also indicated in Table 7. The achieved results have demonstrated that the CTI constraints from Equations (3)–(5) are completely satisfied.

Figure 13 shows the optimal protection characteristic curves of the OC relays in Scenario 4 of the real 22 kV DG-contained DN. Regarding the obtained coordination results of 51P/G and 50P/G functions, Relay 1 represents the OC protection function embedded into the REC Can-Thanh 163 recloser; Relay 2 represents the OC protection function integrated into the REC Can Thanh–Hao Vo recloser; and Relay 3 indicates the OC protection function used to control the REC Can-Thanh 36 OCR recloser. When the 3ph-G fault occurs at Bus 3, the maximum 3ph-G fault current is 2.9 kA as indicated in Table 3, so the primary operation time of the REC Can-Thanh 163 OCR is 0.01 s. The backup operation times of the REC Can-Thanh Hao-Vo OCR and the REC Can-Thanh 36 OCR are about 0.31~0.33 s and 0.63~0.65 s, respectively, according to results of three different algorithms as seen in the table and Figure 13. The backup operation time of the CB GEN OCR is about 0.35 s. Additionally,I_{trip} represents the tripping-current threshold of 50P/G

protection functions of the REC Can-Thanh 163 OCR. By further considering the REC Can-Thanh 163 OCR, the tripping current I_f of its 50G function is set to 2640 A as shown in Table 7. Thus, this tripping current is considered as a terminated point of the inverse-time characteristic curve of the 51G function in the same REC Can-Thanh 163 OCR. Similarly, the tripping current I_f of the 50G function of the REC Can-Thanh Hao-Vo OCR which is 2980 A is considered as a finishing point of the inverse-time characteristic curve of its 51G function, as clearly illustrated by the curve of Relay 2, i.e., the red curves in Figure 13.

Table 7. Optimal protection coordination results of the OCRs in Scenario 4 and their tripping time when the fault is at Bus 3.

The OCRs	50P		50G		51P				51G			
						GA	GSA	PSO-GSA		GA	GSA	PSO-GSA
The REC Can-Thanh 36 OCR	I_f	18,791 A	I_f	20,376 A	A	10.84	42.61	15.58	A	21.36	70.52	149.95
					B	1.24	2.39	1.47	B	2.21	2.40	2.50
					C	1.08	0.39	1.12	C	0.94	0.60	0.08
	$t_{trip}^{defined}$	0.01s	$t_{trip}^{defined}$	0.01 s	TDS	0.13	0.14	0.12	TDS	0.19	0.09	0.05
					The tripping time of the relay for the typical fault at Bus 3:							
					t_{trip}	0.64 s	0.63 s	0.65 s	t_{trip}	0.64 s	0.63 s	0.65 s
The REC Can-Thanh–Hao-Vo OCR	I_f	1798 A	I_f	2980 A	A	8.43	72.23	0.01	A	18.43	77.10	1.52
					B	2.42	2.44	0.02	B	2.31	2.37	1.83
					C	0.50	0.62	0.29	C	0.97	0.77	0.01
	$t_{trip}^{defined}$	0.01 s	$t_{trip}^{defined}$	0.01 s	TDS	0.26	0.05	0.50	TDS	0.12	0.04	1.16
					The tripping time of the relay for the typical fault at Bus 3:							
					t_{trip}	0.32 s	0.31 s	0.33 s	t_{trip}	0.32 s	0.31 s	0.33 s
The REC Can-Thanh 163 OCR	I_f	1672 A	I_f	2640 A	A	1.10	53.82	0.01	A	1.93	39.27	0.01
					B	1.73	1.87	0.71	B	2.37	2.28	1.31
					C	0.00	0.65	0.01	C	0.11	0.77	0.00
	$t_{trip}^{defined}$	0.01 s	$t_{trip}^{defined}$	0.01 s	TDS	0.04	0.01	0.52	TDS	0.03	0.01	2.98
					The tripping time of the relay for the typical fault at Bus 3:							
					t_{trip}	0.01 s	0.01 s	0.01 s	t_{trip}	0.01 s	0.01 s	0.01 s
A CB GEN OCR	I_f	816 A	I_f	910 A	A	4.39	57.46	0.01	A	0.23	67.95	0.01
					B	2.41	2.17	2.50	B	2.45	2.24	2.25
					C	1.18	0.59	0.05	C	0.76	0.80	0.80
	$t_{trip}^{defined}$	0.01 s	$t_{trip}^{defined}$	0.01 s	TDS	0.09	0.01	7.16	TDS	0.35	0.01	0.45
					The tripping time of the relay for the typical fault at Bus 3:							
					t_{trip}	0.35 s	0.32 s	0.35 s	t_{trip}	0.35 s	0.32 s	0.35 s

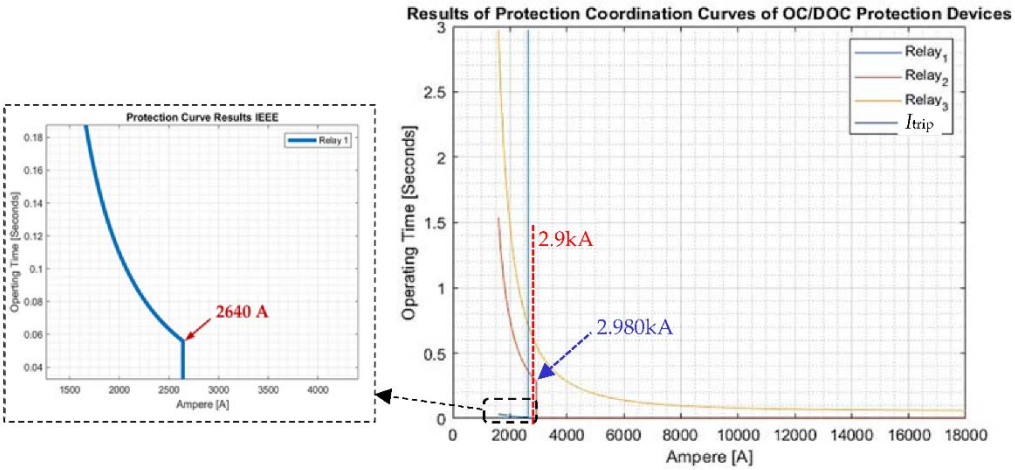

(**a**) The OC protection coordination results of 50G and 51G functions are obtained by the GSA.

Figure 13. *Cont.*

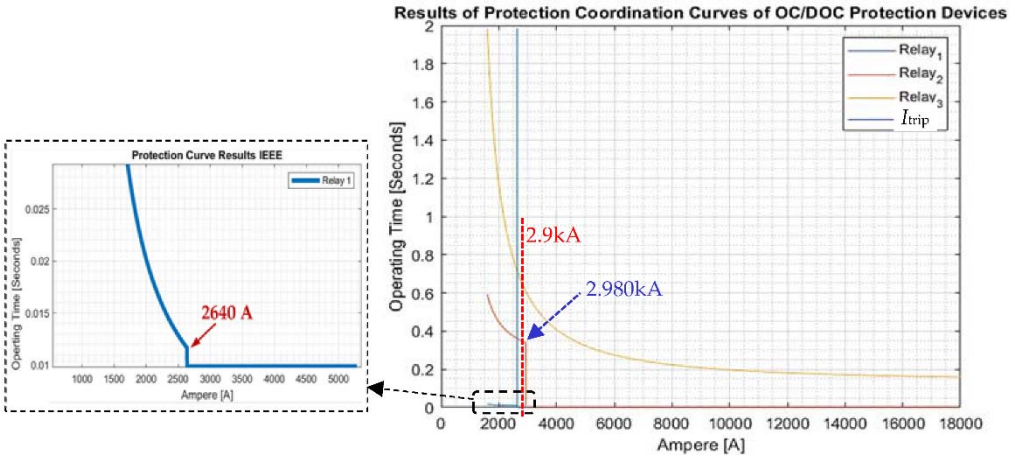

(**b**) The OC protection coordination results of 50G and 51G functions are obtained by the hybrid PSO-GSA.

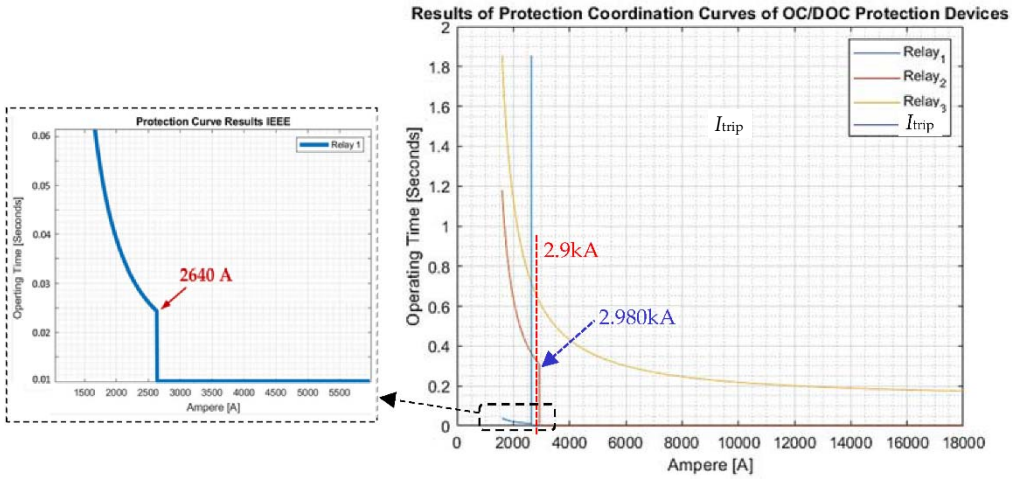

(**c**) The OC protection coordination results of 50G and 51G functions are obtained by the GA.

Figure 13. Optimal protection characteristic curves of the OC relays in Scenario 4 of the 22 kV distribution system.

In summary, the optimal protection coordination results of the related OCRs regarding four different operation scenarios of the real 22 kV DG-based distribution system have been analyzed and validated in this section. These relay coordination results of Scenarios 1, 2, 3 and 4 can be briefly concluded as follows.

- Three meta-heuristic algorithms, GSA, hybrid PSO-GSA and GA have efficiently solved the adaptable and scalable protection coordination problem of the OCRs in the DG-integrated DN as demonstrated in Figures 11–13. The GSA can be a better optimization solution than others because its processing time is quite fast and the difference in the tripping time between the desired one and the calculated one of the related OCRs for Scenarios 1, 2, 3 and 4 is also small as indicated in Table 8. Moreover, although the computation time of the GA is the fastest, the tripping time difference between the desired one and the calculated one of the GA is higher than that of the GSA.
- By applying the proposed ASPC approach for the OCRs, the optimal setting parameters of 50P, 50G, 51P, and 51G protection functions in the same OCR have been properly calculated and updated by the SCADA system whenever the 22 kV DG-integrated DN topology is changed by the faults.
- For each scenario of the DN, a 3ph-G fault has been assumed to occur at the remote end of the feeder, which is the basis to evaluate the obtained relay coordination results. The CTI constraints have been checked for both the OCR pairs and the OCR triples. More

clearly, the primary and backup operation times of the related OCRs regarding the 3ph-G fault at the remote end of the feeder have been already analyzed in Tables 4–7.

Table 8. Comparison in the calculated tripping time of the related OCRs and the computation time of GA, GSA and hybrid PSO-GSA algorithms for Scenarios 1, 2, 3 and 4.

(a) Scenario 1							
Overcurrent relays	Desired tripping time	Calculated tripping time (in seconds) of the related OCRs for the 3ph-G fault at Bus 5 of Scenario 1			Computation time (in seconds) of the optimization algorithms		
		GA	GSA	Hybrid PSO-GSA	GA	GSA	Hybrid PSO-GSA
The REC Can-Thanh 163 OCR	0.01 s	0.01 s	0.01 s	0.01 s	5 s	8 s	14 s
The REC Hao-Vo OCR	0.31 s	0.32 s	0.31 s	0.31 s			
The 471 Hao-Vo OCR	0.61 s	0.62 s	0.61 s	0.62 s			
The highest difference in the tripping time between the desired one and the calculated one among the OCRs		0.01 s	0 s	0.01 s			
(b) Scenario 2							
Overcurrent relays	Desired tripping time	Calculated tripping time (in seconds) of the related OCRs for the 3ph-G fault at Bus 3 of Scenario 2			Computation time (in seconds) of the optimization algorithms		
		GA	GSA	Hybrid PSO-GSA	GA	GSA	Hybrid PSO-GSA
The REC Can-Thanh 163 OCR	0.01 s	0.01 s	0.01 s	0.01 s	6 s	7 s	24 s
The REC Can-Thanh Hao-Vo OCR	0.31 s	0.33 s	0.32 s	0.33 s			
The REC Can-Thanh 36 OCR	0.61 s	0.65 s	0.62 s	0.65 s			
The highest difference in the tripping time between the desired one and the calculated one among the OCRs		0.04 s	0.01 s	0.04 s			
(c) Scenario 3							
Overcurrent relays	Desired tripping time	Calculated tripping time (in seconds) of the related OCRs for the 3ph-G fault at Bus 3 of Scenario 3			Computation time (in seconds) of the optimization algorithms		
		GA	GSA	Hybrid PSO-GSA	GA	GSA	Hybrid PSO-GSA
The REC Can-Thanh 163 OCR	0.01 s	0.01 s	0.01 s	0.01 s	3 s	6 s	7 s
The CB GEN OCR	0.31 s	0.35 s	0.32 s	0.35 s			
The highest difference in the tripping time between the desired one and the calculated one among the OCRs		0.04 s	0.01 s	0.04 s			
(d) Scenario 4							
Overcurrent relays	Desired tripping time	Calculated tripping time (in seconds) of the related OCRs for the 3ph-G fault at Bus 3 of Scenario 4			Computation time (in seconds) of the optimization algorithms		
		GA	GSA	Hybrid PSO-GSA	GA	GSA	Hybrid PSO-GSA
The REC Can-Thanh 163 OCR	0.01 s	0.01 s	0.01 s	0.01 s	5 s	7.8 s	16 s
The REC Can-Thanh Hao-Vo OCR	0.31 s	0.32 s	0.31 s	0.33 s			
The CB GEN OCR	0.31 s	0.35 s	0.32 s	0.35 s			
The REC Can-Thanh 36 OCR	0.61 s	0.64 s	0.63 s	0.65 s			
The highest difference in the tripping time between the desired one and the calculated one among the OCRs		0.04 s	0.02 s	0.04 s			

5. Conclusions

The protection coordination of OCRs becomes more complicated when a distribution network allows high penetration of DGs. Therefore, this paper has proposed an adaptive and scalable protection coordination (ASPC) system for the OCRs in the DG-based DN with two main performance stages. The first stage is to improve the reliability of fault-current calculation results through determining the min-max confidence interval of fault current for each different fault type including 3ph-G, 2ph-G, ph-ph, and 1ph-G faults. The maximum and minimum confidence thresholds of fault current are used to select tripping and pick-up thresholds of definite-time and inverse-time OC functions in the same OCR, respectively. This contribution is to increase the scalability of the relay protection coordination system. In addition, the proposed ASPC approach for the OCRs has high adaptability to different fault current contributions from IBDGs and RBDGs and the available 'on-grid' and 'off-grid' operation modes for these DG units. The second stage is to calculate the A, B, and C certain coefficients and the Time-Dial-Setting (TDS) multiplier for the inverse-time OC functions in the OCR. Three common algorithms, GSA, hybrid PSO-GSA and GA, have been used to find the optimal setting parameters of the OCRs that are satisfied with all coordination constraint conditions. Moreover, the relay coordination results have shown an effective protection combination of the definite-time OC functions (50P and 50G) and the inverse-time OC functions (51P and 51G) in the same OCR to get the adaptable and scalable DN protection system. A real 22 kV DG-integrated distribution network has been simulated by ETAP software to analyze the min-max fault-current values of each fault type. In other words, this real 22 kV DN is used as a test-bed to validate the relay coordination results obtained by the ASPC system. The relay coordination results also show the visibility and superiority of the GSA because it has the fast computation time and the highest stability in comparison with the hybrid PSO-GSA and the GA. The tripping time difference between the desired one and the calculated one of the GSA is also the lowest. Last but not least, it could be interesting that this study has presented the protection coordination results of the related OCRs corresponding to all possible FISR plans of the DG-contained DN after a typical fault is cleared.

Author Contributions: D.M.B., T.P.N., and H.N. contribute conceptualization, methodology, and writing—review and editing of the paper. P.D.L. contributes investigation, data collection and analysis, software, and writing—original draft preparation of the paper. All authors have read and agreed to the published version of the manuscript.

Funding: This research was funded by the Ministry of Education and Training (MOET) and Vietnamese-German University (VGU), a grant number of B2020-VGU-01 and an issued number of 103/QĐ-BGDDT by 21st February 2020.

Institutional Review Board Statement: Not applicable.

Informed Consent Statement: Not applicable.

Acknowledgments: The authors sincerely thank to the Ministry of Education and Training (MOET), Vietnamese-German University (VGU), and Ho Chi Minh City Power Corporation for data supply, administrative and technical support in this research paper.

Conflicts of Interest: The authors declare no conflict of interest.

References

1. Bui, D.M.; Lien, K.Y.; Yu, S.L.; Chen, Y.C.; Lu, C.M.; Chan, C.M.; Chang, Y.R. Investigate dynamic and transient charac-teristics of microgrid operation and develop a fast-scalable-adaptable algorithm for fault protection system. *Electr. Power Syst. Res.* **2015**, *120*, 214–233. [CrossRef]
2. Bui, D.M.; Chen, S.L. Fault protection solutions appropriately proposed for ungrounded low-voltage AC microgrids: Review and proposals. *Renew. Sustain. Energy Rev.* **2017**, *75*, 1156–1174. [CrossRef]
3. Lien, K.-Y.; Bui, D.M.; Chen, S.-L.; Zhao, W.-X.; Chang, Y.-R.; Lee, Y.-D.; Jiang, J.-L. A novel fault protection system using communication-assisted digital relays for AC microgrids having a multiple grounding system. *Int. J. Electr. Power Energy Syst.* **2016**, *78*, 600–625. [CrossRef]

4. Parhizi, S.; Lotfi, H.; Khodaei, A.; Bahramirad, S. State of the art in research on microgrids: A review. *IEEE Access.* **2015**, *3*, 890–925. [CrossRef]
5. Esreraig, M.; Mitra, J. Microgrid protection using system observer and minimum measurement set. *Int. Trans. Electr. Energy Syst.* **2014**, *25*, 607–622. [CrossRef]
6. Bui, D.M. Simplified and automated fault-current calculation for fault protection system of grid-connected low-voltage AC microgrids. *Int. J. Emerg. Electr. Power Syst.* **2017**, *18*, 2. [CrossRef]
7. Laaksonen, H. Protection Principles for Future Microgrids. *IEEE Trans. Power Electron.* **2010**, *25*, 2910–2918. [CrossRef]
8. Esreraig, M.; Lasseter, R.H. Microgrids. In Proceedings of the IEEE Power Engineering Society Winter Meeting, Singapore, 23–27 January 2002; pp. 27–31.
9. Firouz, Y.; Lobry, J.; Vallée, F.; Durieux, O. Numerical comparison of the effects of different types of distributed gener-ation units on overcurrent protection systems in MV distribution grid. *Int. J. Renew. Energy* **2014**, *69*, 271–283.
10. Le, D.P.; Bui, D.M.; Ngo, C.C.; Le, A.M.T. FLISR Approach for Smart Distribution Networks Using E-Terra Soft-ware—A Case Study. *Energies* **2018**, *11*, 3333. [CrossRef]
11. Le, P.D.; Bui, D.M.; Ngo, C.C.; Nguyen, T.P.; Huynh, C.P.; Doan, N.M. A Proposed FLISR Approach for Distribution Networks with Distributed Generators. *IEEE Inter. Con. Power Energy* **2020**, 125–130. [CrossRef]
12. Chabanloo, R.; Abyaneh, H.; Agheli, A.; Rastegar, H. Overcurrent relays coordination considering transient behaviour of fault current limiter and distributed generation in distribution power network. *IET Gener. Transm. Distrib.* **2011**, *5*, 903–911. [CrossRef]
13. Pandi, V.R.; Zeineldin, H.H.; Xiao, W. Determining Optimal Location and Size of Distributed Generation Resources Considering Harmonic and Protection Coordination Limits. *IEEE Trans. Power Syst.* **2012**, *28*, 1245–1254. [CrossRef]
14. Zeineldin, H.; Sharaf, H.; Ibrahim, D.; El-Zahab, E.D.A. Optimal protection coordination for meshed distribution sys-tems with DG using dual setting directional over-current relays. *IEEE Trans. Smart Grid* **2015**, *6*, 115–123. [CrossRef]
15. Mahat, P.; Chen, Z.; Bak-Jensen, B.; Bak, C.L. A Simple Adaptive Overcurrent Protection of Distribution Systems with Distributed Generation. *IEEE Trans. Smart Grid* **2011**, *2*, 428–437. [CrossRef]
16. Walke, S.B.; Nayana, N.J. Methods for relay coordination. In Proceedings of the 2017 International Conference on Computing Meth-Odologies and Communication (ICCMC), Erode, India, 18–19 July 2017; pp. 1027–1032.
17. Huchel, L.; Hatem, H.Z. Planning the coordination of directional overcurrent relays for distribution systems consid-ering DG. *IEEE Trans. Smart Grid* **2015**, *7*, 1642–1649. [CrossRef]
18. Ma, J.; Li, J.; Wang, Z. An adaptive distance protection scheme for distribution system with distributed generation. In Proceedings of the 2010 5th International Conference on Critical Infrastructure (CRIS), Beijing, China, 20–22 September 2010; pp. 1–4. [CrossRef]
19. Javadian, S.; Haghifam, M.-R.; Bathaee, S.; Firoozabad, M.F. Adaptive centralized protection scheme for distribution systems with DG using risk analysis for protective devices placement. *Int. J. Electr. Power Energy Syst.* **2013**, *44*, 337–345. [CrossRef]
20. Zamani, M.A.; Sidhu, T.S.; Yazdani, A. A protection strategy and microprocessor based relay for low-voltage mi-crogrids. *IEEE Trans. Power Deliv.* **2011**, *26*, 1873–1883. [CrossRef]
21. Nikkhajoei, H.; Lasseter, R.H. Microgrid Fault Protection Based on Symmetrical and Differential Current Components. Wisconsin Power Electronics Research Center, Dept. of Elec. and Com., Eng., University of Wisconsin-Madison. 2006. Available online: https://citeseerx.ist.psu.edu/viewdoc/download?doi=10.1.1.375.2266&rep=rep1&type=pdf (accessed on 1 August 2021).
22. Bin, L.; Yongli, L.; Zhiqian, B.; Klimek, A. Design of protection and control scheme for microgrid systems. In Proceedings of the 2009 44th International Universities Power Engineering Conference (UPEC), Glasgow, UK, 1–4 September 2009; pp. 1–5.
23. Best, R.J.; Morrow, D.J.; Crossley, P.A. Communication assisted protection selectivity for reconfigurable and islanded power networks. In Proceedings of the 2009 44th International Universities Power Engineering Conference (UPEC), Glasgow, UK, 1–4 September 2009; pp. 1–5.
24. Polajzer, B.; Pintaric, M.; Roser, M.; Stumberger, G. Protection of MV Closed-Loop Distribution Networks with Bi-Directional Overcurrent Relays and GOOSE Communications. *IEEE Access* **2019**, *7*, 165884–165896. [CrossRef]
25. Asadi, M.R.; Kouhsari, S.M. Optimal overcurrent relays coordination using particle-swarm-optimization methodology. In Proceedings of 2009 IEEE/PES Power Systems Conference and Exposition, Seattle, WA, USA, 15–18 March 2009; pp. 1–7.
26. Albrecht, R.E.; Nisja, M.J.; Feero, W.E.; Rockefeller, G.D.; Wagner, C.L. Digital Computer Protective Device Co-ordination Program I-General Program Description. *IEEE Trans. Power Appar. Syst.* **1964**, *83*, 402–410. [CrossRef]
27. Jenkins, L.; Khincha, H.; Shivakumar, S.; Dash, P. An application of functional dependencies to the topological analysis of protection schemes. *IEEE Trans. Power Deliv.* **1992**, *7*, 77–83. [CrossRef]
28. Urdaneta, A.J.; Nadira, R.; Jimenez, L.G.P. Optimal coordination of directional overcurrent relays in interconnected power systems. *IEEE Trans. Power Deliv.* **1988**, *3*, 903–911. [CrossRef]
29. Mohammadi, R.; Abyaneh, H.A.; Rudsari, H.M.; Fathi, S.H.; Rastegar, H. Overcurrent Relays Coordination Considering the Priority of Constraints. *IEEE Trans. Power Deliv.* **2011**, *26*, 1927–1938. [CrossRef]
30. Noghabi, A.S.; Mashhadi, H.R.; Sadeh, J. Optimal Coordination of Directional Overcurrent Relays Considering Different Network Topologies Using Interval Linear Programming. *IEEE Trans. Power Deliv.* **2010**, *25*, 1348–1354. [CrossRef]
31. Moravej, Z.; Adelnia, F.; Abbasi, F. Optimal coordination of directional overcurrent relays using NSGA-II. *Electr. Power Syst. Res.* **2015**, *119*, 228–236. [CrossRef]

32. Thangaraj, R.; Pant, M.; Abraham, A. New mutation schemes for differential evolution algorithm and their application to the optimization of directional over-current relay settings. *Appl. Math. Comput.* **2010**, *216*, 532–544. [CrossRef]
33. Thangaraj, R.; Pant, M.; Deep, K. Optimal coordination of over-current relays using modified differential evolution algorithms. *Eng. Appl. Artif. Intell.* **2010**, *23*, 820–829. [CrossRef]
34. Sirinivas, S.P.T.; Swarup, K.S.H. A new mixed integer linear programing formulation for protection relay coordination using disjunctive inequalities. *IEEE Power Energy Technol. Syst. J.* **2019**, *6*, 104–112. [CrossRef]
35. Hui, Y.; Fushuan, W.; Zhuhai, G.L. Optimal coordination of overcurrent relays in distribution systems with distributed generators based on differential evolution algorithm. *Eur. Trans. Elect. Power* **2013**, *23*, 1–12.
36. Yazdaninejadi, A.; Nazarpour, D.; Talavat, V. Optimal coordination of dual-setting directional over-current relays in multi-source meshed active distribution networks considering transient stability. *IET Gener. Transm. Distrib.* **2018**, *13*, 157–170. [CrossRef]
37. Saleh, K.; Zeineldin, H.H.; Al-Hinai, A.; El-Saadany, E.F. Optimal Coordination of Directional Overcurrent Relays Using a New Time–Current–Voltage Characteristic. *IEEE Trans. Power Deliv.* **2014**, *30*, 537–544. [CrossRef]
38. Dehghanpour, E.; Karegar, H.K.; Kheirollahi, R.; Soleymani, T. Optimal Coordination of Directional Overcurrent Relays in Microgrids by Using Cuckoo-Linear Optimization Algorithm and Fault Current Limiter. *IEEE Trans. Smart Grid* **2016**, *9*, 1365–1375. [CrossRef]
39. Shrivastava, A.; Tripathi, J.M.; Krishan, R.; Parida, S. Optimal Coordination of Overcurrent Relays using Gravitational Search Algorithm with DG Penetration. *IEEE Trans. Ind. Appl.* **2017**, 1. [CrossRef]
40. Kida, A.A.; Gallego, L.A. A high-performance hybrid algorithm to solve the optimal coordination of overcurrent relays in radial distribution networks considering several curve shapes. *Electr. Power Syst. Res.* **2016**, *140*, 464–472. [CrossRef]
41. Bouchekara, H.; Zellagui, M.; Abido, M. Optimal coordination of directional overcurrent relays using a modified electromagnetic field optimization algorithm. *Appl. Soft Comput.* **2017**, *54*, 267–283. [CrossRef]
42. Moirangthem, J.; Krishnanand, K.R.; Dash, S.S.; Ramaswami, R. Adaptive differential evolution algorithm for solving non-linear coordination problem of directional overcurrent relays. *IET Gener. Transm. Distrib.* **2013**, *7*, 329–336. [CrossRef]
43. Shih, M.Y.; Salazar, C.A.C.; Enriquez, A.C. Adaptive directional overcurrent coordination using ant colony opti-mization. *IET Gener. Transm. Distrib.* **2015**, *9*, 1240–2049.
44. Bedekar, P.P.; Bhide, S.R. Optimum Coordination of Directional Overcurrent Relays Using the Hybrid GA-NLP Approach. *IEEE Trans. Power Deliv.* **2010**, *26*, 109–119. [CrossRef]
45. Sueiro, J.A.; Diaz-Dorado, E.; Mguez, E.; Cidrs, J. Coordination of directional overcurrent relay using evolutionary algorithm and linear programming. *Elect. Power Energy Syst.* **2012**, *42*, 299–305. [CrossRef]
46. Al-basri, F.A.; Al-roomi, A.R.; Talaq, J.H. Optimal coordination of directional overcurrent relays using biogeogra-phy-based optimization algorithms. *IEEE Trans. Power Del.* **2015**, *30*, 1810–1820. [CrossRef]
47. Saberi, H.; Amraee, T. Coordination of directional over-current relays in active distribution networks using generalized benders decomposition. *IET Gener. Transmiss. Distrib.* **2017**, *11*, 4078–4086. [CrossRef]
48. Saha, D.; Datta, A.; Das, P. Optimal coordination of directional overcurrent relays in power systems using Symbiotic Organism Search Optimisation technique. *IET Gener. Transm. Distrib.* **2016**, *10*, 2681–2688. [CrossRef]
49. Amraee, T. Coordination of Directional Overcurrent Relays Using Seeker Algorithm. *IEEE Trans. Power Deliv.* **2012**, *27*, 1415–1422. [CrossRef]
50. Ezzeddine, M.; Kaczmarek, R.; Iftikhar, M.U. Coordination of directional overcurrent relays using GA novel method to select their settings. *IET Gener. Transmiss. Distrib.* **2011**, *5*, 743–750. [CrossRef]
51. Baghaee, H.R.; Mirsalim, M.; Gharehpetian, G.B.; Talebi, H.A. MOPSO/FDMT-based Pareto-optimal solution for co-ordination of overcurrent relays in interconnected networks and multi-DER microgrids. *IET Gener. Transmiss. Distrib.* **2018**, *12*, 2871–2886. [CrossRef]
52. Shih, M.Y.; Conde, A.; Leonowicz, Z.; Martirano, L. An Adaptive Overcurrent Coordination Scheme to Improve Relay Sensitivity and Overcome Drawbacks due to Distributed Generation in Smart Grids. *IEEE Trans. Ind. Appl.* **2017**, *53*, 5217–5228. [CrossRef]
53. Nascimento, J.P.; Brito, N.S.; Souza, B.A. An adaptive overcurrent protection system applied to distribution systems. *Comput. Electr. Eng.* **2020**, *81*, 106545. [CrossRef]
54. Samadi, A.; Chabanloo, R.M. Adaptive coordination of overcurrent relays in active distribution networks based on independent change of relays' setting groups. *Int. J. Electr. Power Energy Syst.* **2020**, *120*, 106026. [CrossRef]
55. Ates, Y.; Uzunoglu, M.; Karakas, A.; Boynuegri, A.R.; Nadar, A.; Dag, B. Implementation of adaptive relay coordination in distribution systems including distributed generation. *J. Clean. Prod.* **2016**, *112*, 2697–2705. [CrossRef]
56. Ahmadi, S.; Karami, H.; Sanjari, M.; Tarimoradi, H.; Gharehpetian, G. Application of hyper-spherical search algorithm for optimal coordination of overcurrent relays considering different relay characteristics. *Int. J. Electr. Power Energy Syst.* **2016**, *83*, 443–449. [CrossRef]
57. IEEE Power and Energy Society. "C37.112-2018—IEEE Standard for Inverse-Time Characteristics Equations for Overcurrent Relays—IEEE Standard; 2018; Volume C37. Available online: https://ieeexplore.ieee.org/document/8635630 (accessed on 1 August 2021).
58. IEC. *Electrical Relays-Part 3: Single Input Energizing Quantity Measuring Relays with Dependent or Independent Time*; International Electrotechnical Commission: Geneva, Switzerland, 1989; pp. 60255–60263.

59. Majumder, R.; Dewadasa, M.; Ghosh, A.; Ledwich, G.; Zare, F. Control and protection of a microgrid connected to utility through back-to-back converters. *Electr. Power Syst. Res.* **2011**, *81*, 1424–1435. [CrossRef]
60. Dewadasa, M.; Ghosh, A.; Ledwich, G.; Wishart, M. Fault isolation in distributed generation connected distribution networks. *IET Gener. Transm. Distrib.* **2011**, *5*, 1053–1061. [CrossRef]
61. Darabi, A.; Bagheri, M.; Gharehpetian, G.B. Highly sensitive microgrid protection using overcurrent relays with a novel relay characteristic. *IET Renew. Power Gener.* **2020**, *14*, 1201–1209. [CrossRef]
62. Jamali, S.; Borhani-Bahabadi, H. Recloser time–current–voltage characteristic for fuse saving in distribution networks with DG. *IET Gener. Transm. Distrib.* **2017**, *11*, 272–279. [CrossRef]
63. Jamali, S.; Borhani-Bahabadi, H. Self-Adaptive Relaying Scheme of Reclosers for Fuse Saving in Distribution Networks with DG. *Int. J. Power Energy Res.* **2017**, *1*. [CrossRef]
64. Kılıçkıran, H.C.; Akdemir, H.; Sengor, I.; Kekezoğlu, B.; Paterakis, N.G. A Non-Standard Characteristic Based Protection Scheme for Distribution Networks. *Energies* **2018**, *11*, 1241. [CrossRef]
65. Alam, M.N.; Gokaraju, R.; Chakrabarti, S. Protection coordination for networked microgrids using single and dual setting overcurrent relays. *IET Gener. Transm. Distrib.* **2020**, *14*, 2818–2828. [CrossRef]
66. Mahindara, V.R.; Rodriguez, D.F.C.; Pujiantara, M.; Priyadi, A.; Purnomo, M.H.; Muljadi, E. Practical Challenges of Inverse and Definite-Time Overcurrent Protection Coordination in Modern Industrial and Commercial Power Distribution System. *IEEE Trans. Ind. Appl.* **2020**, *57*, 187–197. [CrossRef]
67. Bedekar, P.P.; Bhide, S.R. Optimum coordination of overcurrent relay timing using continuous genetic algorithm. *Expert Syst. Appl.* **2011**, *38*, 11286–11292. [CrossRef]
68. Gokhale, S.; Kale, V. An application of a tent map initiated Chaotic Firefly algorithm for optimal overcurrent relay coordination. *Int. J. Electr. Power Energy Syst.* **2016**, *78*, 336–342. [CrossRef]
69. Zeineldin, H.; El-Saadany, E.; Salama, M. Optimal coordination of overcurrent relays using a modified particle swarm optimization. *Electr. Power Syst. Res.* **2006**, *76*, 988–995. [CrossRef]
70. Uthitsunthorn, D.; Pao-La-Or, P.; Kulworawanichpong, T. Optimal overcurrent relay coordination using artificial bees colony algorithm. In Proceedings of the 8th Electrical Engineering/Electronics, Computer, Telecommunications and Information Technology (ECTI) Association of Thailand-Conference, Khon Kaen, Thailand, 17–19 May 2011; pp. 901–904.
71. Alaee, P.; Amraee, T. Optimal Coordination of Directional Overcurrent Relays in Meshed Active Distribution Network Using Imperialistic Competition Algorithm. *J. Mod. Power Syst. Clean Energy* **2021**, *9*, 416–422. [CrossRef]
72. Singh, M.; Panigrahi, B.; Abhyankar, A. Optimal coordination of directional over-current relays using Teaching Learning-Based Optimization (TLBO) algorithm. *Int. J. Electr. Power Energy Syst.* **2013**, *50*, 33–41. [CrossRef]
73. Barzegari, M.; Bathaee, S.; Alizadeh, M. Optimal coordination of directional overcurrent relays using harmony search algorithm. In Proceedings of the IEEE Transactions on Power Delivery, Prague, Czech Republic, 16–19 May 2010; pp. 321–324. [CrossRef]
74. Benabid, R.; Zellagui, M.; Chaghi, A.; Boudour, M. Application of Firefly Algorithm for Optimal Directional Overcurrent Relays Coordination in the Presence of IFCL. *Int. J. Intell. Syst. Appl.* **2014**, *6*, 44–53. [CrossRef]
75. Blackburn, J.L.; Domin, T.J. *Protective Relaying: Principles and Applications*; CRC Press: Boca Raton, FL, USA, 2015.
76. Jalilian, A.; Hagh, M.T.; Hashemi, S.M. An Innovative Directional Relaying Scheme Based on Postfault Current. *IEEE Trans. Power Deliv.* **2014**, *29*, 2640–2647. [CrossRef]
77. Eissa, M.M. Current directional protection technique based on polarizing current. *Int. J. Electr. Power Energy Syst.* **2013**, *44*, 488–494. [CrossRef]
78. Ukil, A.; Deck, B.; Shah, V.H. Current-Only Directional Overcurrent Relay. *IEEE Sensors J.* **2010**, *11*, 1403–1404. [CrossRef]
79. Ukil, A.; Deck, B.; Shah, V.H. Current-Only Directional Overcurrent Protection for Distribution Automation: Challenges and Solutions. *IEEE Trans. Smart Grid* **2012**, *3*, 1687–1694. [CrossRef]
80. Nojavan, M.; Seyedi, H.; Mehdinejad, M. A novel scheme for current-only directional overcurrent relay. *Int. J. Electr. Power Energy Syst.* **2016**, *82*, 252–263. [CrossRef]
81. Le, P.D.; Bui, D.M.; Ngo, C.C.; Huynh, C.D.; Nguyen, T.H. Effectively Determine Confidence Intervals of Bus Voltages Served for Setting Overcurrent Relays in Distribution Networks. In Proceedings of the IEEE International Conference on Power and Energy (PECon), Penang, Malaysia, 7–8 December 2020. [CrossRef]
82. Bui, D.M.; Le, P.D.; Cao, M.T.; Pham, T.T.; Pham, D.A. Accuracy improvement of various short-term load forecasting models by a novel and unified statistical data-filtering method. *Int. J. Green Energy* **2020**, *17*, 382–406. [CrossRef]
83. Distribution Network Analysis Functions (DNAF) Analyst and Configuration Editor User's Guide. ALSTOM Grid Inc.: Redmond, WA, USA, 2014.
84. Teng, J.H.; Lin, W.M. Current-based power flow solutions for distribution systems. In Proceedings of the IEEE Intetnatioal Conference Power System Technology, Beijing, China, 5–9 December 1994; pp. 414–418.
85. Chen, T.-H.; Chen, M.-S.; Hwang, K.-J.; Kotas, P.; Chebli, E. Distribution system power flow analysis-a rigid approach. *IEEE Trans. Power Deliv.* **1991**, *6*, 1146–1152. [CrossRef]
86. Teng, J.-H. A direct approach for distribution system load flow solutions. *IEEE Trans. Power Deliv.* **2003**, *18*, 882–887. [CrossRef]
87. Samoylenko, V.O.; Korkunova, O.L.; Pazderin, A.; Novikov, N.N. Overcurrent protection adjustment when connecting synchronous generation to power supply systems. In Proceedings of the IEEE International Conference on Industrial Technology (ICIT), Seville, Spain, 17–19 March 2015; pp. 2368–2373. [CrossRef]

88. *1547.2-2008-IEEE Application Guide for IEEE Standard 1547™, IEEE Standard for Interconnecting Distributed Resources with Electric Power Systems*; IEEE Standards: Piscataway, NJ, USA, 2009; pp. 1–217. [CrossRef]
89. Sortomme, E.; Mapes, G.J.; Foster, B.A.; Venkata, S.S. Fault analysis and protection of a microgrid. In Proceedings of the 40th North American Power Symposium, Calgary, AB, Canada, 28–30 September 2008; pp. 1–6.
90. Johnston, W.; Katiraei, F. *Impact and Sensitivity Studies of PV Inverters Contribution to Faults based on Generic PV In-Verter Models*; Ontario Grid Connection Study 2012; Canadian Solar Industries Association/L'Association des Industries Solaires du Canada: Ottawa, ON, Canada, 2012.
91. IEEE. *IEEE Recommended Practice for Protection and Coordination of Industrial and Commercial Power Systems (IEEE Buff Book)*; IEEE Standards: Piscataway, NJ, USA, 2008; pp. 1–710. [CrossRef]
92. Geidl, M. *Protection of Power Systems with Distributed Generation: State of the Art*; Swiss Federal Institute of Technology (ETH): Zurich, Switzerland, 2005. [CrossRef]
93. Horowitz, S.; Phadke, A. Power System Relaying [Books and Reports]. *IEEE Power Eng. Rev.* **1993**, *13*, 38. [CrossRef]
94. Rashedi, E.; Nezamabadi-Pour, H.; Saryazdi, S. GSA: A Gravitational Search Algorithm. *Inf. Sci.* **2009**, *179*, 2232–2248. [CrossRef]
95. Kennedy, J.; Eberhart, R. Particle swarm optimization. In Proceedings of the IEEE International Conference Neural Networks IV, Perth, Australia, 27 November–1 December 1995; pp. 1942–1948. [CrossRef]
96. Srivastava, A.; Tripathi, J.M.; Mohanty, S.R.; Panda, B. Optimal Over-Current Relay Coordination with Distributed Generation Using Hybrid Particle Swarm Optimization–Gravitational Search Algorithm. *Electr. Power Compon. Syst.* **2016**, *44*, 1–12. [CrossRef]
97. Ahmad, M.; Ali, W.; Farooq, H.; Jamil, M.; Ali, M.; Rehman, A.U. Solving the Problem of Economic Load Dispatch for a Small Scale Power System Using a Novel Hybrid PSO-GSA Algorithm. In Proceedings of the 2018 International Symposium on Recent Advances in Electrical Engineering (RAEE), Islambad, Pakistan, 17–18 October 2018; pp. 1–6. [CrossRef]
98. Goldberg, D.E. *Genetic Algorithms in Search, Optimization, and Machine Learning*; Dorling Kindersley (India) Pvt. Ltd.: New Delhi, India, 2008.
99. Asadi, M.R.; Askarian Abyaneh, H.; Mahmoodan, M.; Naghizadeh, R.A.; Koochaki, A. Optimal overcurrent relays coordination using genetic algorithm. In Proceedings of the 2008 11th International Conference on Optimization of Electrical and Electronic Equipment, Brasov, Romania, 22–24 May 2008; pp. 197–202.